Journal of Computational and Applied Mathematics 489 (2027) 117914

Contents lists available at ScienceDirect

# Journal of Computational and Applied Mathematics

journal homepage: www.elsevier.com/locate/cam

# New approach for constructing edge B–spline–like basis functions for $C^1$ and $C^2$ splines over triangulations

Marjeta Knez [a,b,*], Matija Šteblaj [a]

[a] Faculty of Mathematics and Physics, University of Ljubljana, Jadranska 19, 1000 Ljubljana, Slovenia
[b] Institute of Mathematics, Physics and Mechanics, Jadranska 19, 1000 Ljubljana, Slovenia

ARTICLE INFO

*Keywords:*
Bernstein–Bézier form
$C^r$ Splines over triangulations
B–Spline–like basis
Control triangles
Subdivision

ABSTRACT

Splines over triangulations provide a flexible and effcient way to approximate bivariate functions defined over domains, partitioned by triangles. One of the important challenges is the construction of locally supported non-negative basis functions that form a partition of unity, i.e., B–spline–like basis functions. Due to smoothness conditions that depend on the geometry of the triangulation, spline basis functions are typically divided into three groups: triangle, vertex, and edge functions. While the construction of triangle and vertex basis splines is well developed, the computation of non-negative edge basis splines of general degree that form a partition of unity has so far been addressed only for $C^1$ continuous splines, using a completely algebraic approach, with no explicit geometric interpretation ([7]). In this paper a novel approach is presented that extends the control-triangle-based idea known for vertex basis splines and can be geometrically explained and generalized to splines of a higher order of smoothness. The construction is developed on pairs of adjacent triangles forming a strictly convex quadrilateral. Since each smoothness order requires a separate analysis, a detailed study is provided for the $C^1$ and $C^2$ continuous splines of degrees $d \geq 2$ and $d \geq 4$, respectively. Numerical examples are provided to confirm the effectiveness and applicability of the derived construction.

## 1. Introduction

Splines over triangulations provide a geometrically flexible framework for applications in approximation theory, computer-aided geometric design (CAGD) and numerical analysis. Such splines consist of polynomials of total degree less than or equal to a fixed prescribed degree, defined over triangles of a triangulation, and are usually represented using the local Bernstein–Bézier representation (see, e.g., [1, Chapters 2, 5]). The smoothness of a chosen order across the edges of the triangulation is obtained by imposing linear constraints on the coefficients of the Bernstein–Bézier forms over the neighboring triangles. However, the geometric flexibility comes with the price that in general even the dimension of the spline space is not easy to be determined, as it depends on the geometry of the triangulation. There are two standard approaches to overcome this difficulty. The first is to consider super-smooth spline spaces, in which higher-order smoothness is imposed at selected vertices or edges of the triangulation (e.g., Argyris splines [2]). The second approach, known as the macro-element technique, defines spline spaces over the triangulation refined by a selected split (e.g. Clough–Tocher splines [3], Powell–Sabin splines [4]).

For both approaches the dimension and the basis splines are determined by finding the minimal determining set that identifies the coefficients in the Bernstein–Bézier form that are free to be chosen, or to specify a collection of interpolation functionals (see, e.g.,

* Corresponding author.
*E-mail addresses:* marjetka.knez@fmf.uni-lj.si (M. Knez), matija.steblaj@fmf.uni-lj.si (M. Šteblaj).

https://doi.org/10.1016/j.cam.2026.117914
Received 26 January 2026; Received in revised form 1 June 2026
Available online 23 June 2026

[1, Chapters 6, 7, 8]), such that the associated interpolation problem has a unique solution in the given spline space. The resulting basis splines generally lack some key properties, such as non-negativity and the partition of unity property.

A locally supported basis composed of non-negative splines forming the partition of unity will be referred to as a *B–spline–like basis*. The construction of such bases has been an active area of research in recent years (see, e.g., [5–9]). A common strategy is to separate the domain points in the minimal determining set to three groups – vertex, edge, and triangle group – which then decomposes the basis to vertex, edge and triangle basis splines. Note, that for certain choices of the degree and the split, some basis groups may be omitted.

The idea for computing vertex basis splines was first introduced in [10] for quadratic $C^1$ Powell–Sabin splines. It is based on assigning a control triangle to each vertex and defining the vertex basis splines using three interpolation functionals associated with the vertices of the control triangle. The use of Bernstein basis polynomials over the control triangles for the definition of vertex basis functions was later introduced by Speleers in [6] in the context of quintic $C^2$ Powell–Sabin splines. There, the interpolation conditions defining the vertex basis functions were derived from the Bernstein basis polynomials associated with the control triangles. The idea was further theoretically developed in [11], where, in addition, relations between Bézier coefficients of polynomials of different degrees corresponding to the same interpolation conditions were established, allowing for an elegant subdivision–based construction that is employed in this paper as well. This control triangle approach, which has also been generalized to higher orders of smoothness, can be found in, e.g., [5,6,8,12–15]. An important advantage of such basis constructions is their natural application to the development of quasi–interpolants; see, e.g., [16] and the references therein.

While the construction of vertex basis splines is well established and geometrically intuitive, the construction of B–spline–like basis functions associated with degrees of freedom belonging to the edges of a triangulation has received comparatively less attention. One of the existing contributions in this direction is the paper [9], in which a construction of $C^1$ continuous edge basis splines is presented. It is shown therein that, in order to achieve locality, the problem can be reduced to the study of such basis splines defined over two neighboring triangles only. The proposed approach is mathematically rigorous and effective, but it is primarily algebraic in nature and lacks a clear geometric interpretation. Consequently, possible extensions to higher orders of smoothness are not apparent.

In general, research on splines of global smoothness $r \geq 2$ is less developed. General approaches for Powell-Sabin splines of arbitrary degree and smoothness are given in [7,11], and some simplex splines approaches for $C^2$ are described in [17,18]. Some $C^2$ constructions and applications can also be found in [19].

Motivated by the idea of extending the control-triangle-based construction to edge basis splines, an entirely new approach for the construction of edge B–spline–like functions is presented in this paper. As in [9], the construction is localized to two triangles $T_1$ and $T_2$ sharing a common edge and forming a strictly convex quadrilateral, and the Bernstein–Bézier representation is employed. The method developed in this paper is based on the selection of two specific control triangles that contain both triangles $T_1$ and $T_2$. The key idea underlying the proposed approach is to identify such control triangles that, after subdividing the Bernstein basis polynomials defined over each control triangle onto $T_1$ and $T_2$, a large number of the resulting Bernstein–Bézier coefficients vanish. Furthermore, a clear separation of candidates for vertex and edge basis splines with the desired properties is possible. Two control triangles are required in order to derive a sufficient number of linearly independent edge basis splines. The proposed construction is entirely geometric in nature and can be applied to derive $C^r$ continuous edge B–spline–like splines of sufficiently high degree. However, since each smoothness order requires a separate analysis, a detailed study is provided for the $C^1$ and $C^2$ continuous cases, which are the most relevant for practical applications.

The remainder of the paper is organized as follows. A short review of Bernstein–Bézier representation for polynomials over triangles together with the notation employed in this work is given in Section 2. In Section 3 splines over two triangles sharing an edge and forming a strictly convex quadrilateral are considered, control triangles are introduced and candidates for vertex and edge B–spline–like basis functions are derived. Derivation of $C^1$ continuous B–spline–like basis functions of degree $d \geq 2$ is given in Section 4 together with numerical examples and a comparison with the basis splines derived in [9]. Section 5 is devoted to the analysis of $C^2$ continuous splines of degree $d \geq 4$. Some notes on edge B–spline–like splines of higher order of smoothness are provided in Section 6, and concluding remarks are given in Section 7.

## 2. Bernstein–Bézier representation of polynomials over a triangle

We denote by $\mathbb{P}_d^1$ the univariate polynomials of degree $d$, and by $\mathbb{P}_d^2$ the bivariate polynomials of total degree $d$. Any $p \in \mathbb{P}_d^1$, observed over the interval $[a,b]$, can be uniquely expressed in a Bernstein–Bézier representation

$$p(x) = \sum_{i=0}^{d} c_i B_i^d(\tfrac{x-a}{b-a}), \quad x \in [a,b], \qquad B_i^d(t) := \binom{d}{i} t^i (1-t)^{d-i}, \quad t \in [0,1].$$

The coefficients $c_i \in \mathbb{R}$, called Bézier coefficients, define control points $((1-\frac{i}{d})a + \frac{i}{d}b, c_i) \in \mathbb{R}^2$, $i = 0,1,\dots,d$, and their *control polygon* determines the shape of the graph of $p$ over the interval $[a,b]$. Bivariate polynomials are naturally observed over triangles. With $T = (\boldsymbol{V}_1, \boldsymbol{V}_2, \boldsymbol{V}_3)$ we denote the triangle with vertices $\boldsymbol{V}_i$, $i = 1,2,3$, and $\triangle_0 := ((1,0),(0,1),(0,0))$ is a so called *unit* triangle. To enumerate the bivariate Bernstein basis polynomials we define the set

$$\mathbb{I}_d := \left\{ \boldsymbol{i} = (i_1, i_2, i_3) \in \mathbb{N}_0^3 : \ |\boldsymbol{i}| = i_1 + i_2 + i_3 = d \right\}$$

consisting of $\binom{d+2}{2}$ multi-indices, which is the dimension of $\mathbb{P}^2_d$. For any $p \in \mathbb{P}^2_d$, its Bernstein–Bézier representation over $\triangle_0$ is of the form

$$p(u,v) = \sum_{\boldsymbol{i}\in\mathbb{I}_d} c_{\boldsymbol{i}} B_{\boldsymbol{i}}^{\triangle,d}(u,v), \quad B_{\boldsymbol{i}}^{\triangle,d}(u,v) := \frac{d!}{i_1!i_2!i_3!} u^{i_1} v^{i_2} (1-u-v)^{i_3}, \quad (u,v) \in \triangle_0, \quad \boldsymbol{i} = (i_1,i_2,i_3) \in \mathbb{I}_d,$$

for some coefficients $c_{\boldsymbol{i}} \in \mathbb{R}$, and this representation allows us to define the control mesh over $\triangle_0$ with control points $\left\{ (\frac{i_1}{d}, \frac{i_2}{d}, c_{\boldsymbol{i}}) : \boldsymbol{i} \in \mathbb{I}_d \right\}$. To define such a representation over a general triangle $T$ we need to express points in $T$ by their barycentric coordinates with respect to $T$. Namely, for $\boldsymbol{X} \in T$, we denote by $\mathrm{Bar}_T(\boldsymbol{X}) = (u_1,u_2,u_3)$ triple of values such that $\boldsymbol{X} = u_1\boldsymbol{V}_1 + u_2\boldsymbol{V}_2 + u_3\boldsymbol{V}_3$ and $u_1+u_2+u_3 = 1$. Barycentric mapping is closely related to the bijective linear mapping

$$\boldsymbol{G}_T : \triangle_0 \to T, \quad \boldsymbol{G}_T(u,v) := u\boldsymbol{V}_1 + v\boldsymbol{V}_2 + (1-u-v)\boldsymbol{V}_3$$

of the triangle $\triangle_0$ into $T$. Namely, for each $\boldsymbol{X} \in T$ the first two barycentric coordinates $(u_1,u_2,u_3) = \mathrm{Bar}_T(\boldsymbol{X})$ are equal to $(u_1,u_2) = \boldsymbol{G}_T^{-1}(\boldsymbol{X})$ and the last one is clearly $u_3 = 1-u_1-u_2$. With this notation the Bernstein–Bézier representation of a polynomial $p$ over a general triangle $T$ is given as

$$p(\boldsymbol{X}) = \sum_{\boldsymbol{i}\in\mathbb{I}_d} c_{\boldsymbol{i}}^T B_{\boldsymbol{i}}^{T,d}(\boldsymbol{X}), \quad B_{\boldsymbol{i}}^{T,d} := B_{\boldsymbol{i}}^{\triangle,d} \circ \boldsymbol{G}_T^{-1}, \tag{1}$$

for some Bézier coefficients $c_{\boldsymbol{i}}^T \in \mathbb{R}$ that together with domain points

$$\boldsymbol{X}_{\boldsymbol{i}}^{T,d} := \boldsymbol{G}_T(\tfrac{i_1}{d}, \tfrac{i_2}{d}) = \tfrac{i_1}{d}\boldsymbol{V}_1 + \tfrac{i_2}{d}\boldsymbol{V}_2 + \tfrac{i_3}{d}\boldsymbol{V}_3, \quad \boldsymbol{i} \in \mathbb{I}_d, \tag{2}$$

define the control mesh with control points $(\boldsymbol{X}_{\boldsymbol{i}}^{T,d}, c_{\boldsymbol{i}}^T)$.

**Remark 1.** To denote the set of Bézier coefficients $\{c_{\boldsymbol{i}} : \boldsymbol{i} \in \mathbb{I}_d\}$, we use the representation with a lower triangular matrix $\boldsymbol{C} = \mathrm{Mat}\Big( (c_{\boldsymbol{i}})_{\boldsymbol{i}\in\mathbb{I}_d} \Big)$, $\boldsymbol{C} \in \mathbb{R}^{(d+1)\times(d+1)}$, such that its element $\boldsymbol{C}(i,j)$ in $i$–th row and $j$–th column (counted from 0 to $d$) equals $\boldsymbol{C}(i,j) = c_{(i-j,j,d-i)}$. Equivalently, $c_{(i_1,i_2,i_3)} = \boldsymbol{C}(d-i_3, i_2)$. In particular, this matrix representation for degrees $d=3$ and $d=4$ equals

$$\begin{bmatrix} c_{(0,0,3)} & 0 & 0 & 0 \\ c_{(1,0,2)} & c_{(0,1,2)} & 0 & 0 \\ c_{(2,0,1)} & c_{(1,1,1)} & c_{(0,2,1)} & 0 \\ c_{(3,0,0)} & c_{(2,1,0)} & c_{(1,2,0)} & c_{(0,3,0)} \end{bmatrix}, \quad \begin{bmatrix} c_{(0,0,4)} & 0 & 0 & 0 & 0 \\ c_{(1,0,3)} & c_{(0,1,3)} & 0 & 0 & 0 \\ c_{(2,0,2)} & c_{(1,1,2)} & c_{(0,2,2)} & 0 & 0 \\ c_{(3,0,1)} & c_{(2,1,1)} & c_{(1,2,1)} & c_{(0,3,1)} & 0 \\ c_{(4,0,0)} & c_{(3,1,0)} & c_{(2,2,0)} & c_{(1,3,0)} & c_{(0,4,0)} \end{bmatrix}.$$

Many essential operations on polynomials, such as evaluation, subdivision and differentiation can be easily applied using the blossoming principle (see [20–22] for more details). Note that the blossom $\mathcal{B}[p] : (\mathbb{R}^2)^d \to \mathbb{R}$ of a polynomial $p$ is independent of the representation of $p$. However, if $p$ is given in the Bernstein–Bézier form (1), its blossom $\mathcal{B}[p]$ can be easily computed using the generalized de Casteljau algorithm, given in Algorithm 1. The following properties are further needed:

1. Let $p \in \mathbb{P}^2_d$. The Bézier coefficients in (1) are equal to $c_{\boldsymbol{i}}^T = \mathcal{B}[p]\Big( \boldsymbol{V}_1^{\langle i_1\rangle}, \boldsymbol{V}_2^{\langle i_2\rangle}, \boldsymbol{V}_3^{\langle i_3\rangle} \Big)$, $\boldsymbol{i} \in \mathbb{I}_d$.
2. Suppose that $T = (\boldsymbol{V}_1, \boldsymbol{V}_2, \boldsymbol{V}_3)$ and $Q = (\boldsymbol{Q}_1, \boldsymbol{Q}_2, \boldsymbol{Q}_3)$ are two triangles and let $p \in \mathbb{P}^2_d$ be given by (1) with $\boldsymbol{C} = \mathrm{Mat}\Big( (c_{\boldsymbol{i}}^T)_{\boldsymbol{i}\in\mathbb{I}_d} \Big)$. The coefficients of the Bernstein–Bézier representation of $p$ over the triangle $Q$ can be computed by

$$c_{\boldsymbol{i}}^Q = \mathcal{B}[p]\Big( \boldsymbol{Q}_1^{\langle i_1\rangle}, \boldsymbol{Q}_2^{\langle i_2\rangle}, \boldsymbol{Q}_3^{\langle i_3\rangle} \Big) = \mathtt{DeCast}\Big( \boldsymbol{C}, \Big( \boldsymbol{Q}_1^{\langle i_1\rangle}, \boldsymbol{Q}_2^{\langle i_2\rangle}, \boldsymbol{Q}_3^{\langle i_3\rangle} \Big), T \Big), \quad \boldsymbol{i} \in \mathbb{I}_d. \tag{3}$$

**Algorithm 1:** de Casteljau algorithm (DeCast).

**Input:** Matrix $\boldsymbol{C}$ with Bézier coefficients $\{c_{\boldsymbol{i}} : \boldsymbol{i} \in \mathbb{I}_d\}$, points $\boldsymbol{X}_1, \boldsymbol{X}_2, \dots, \boldsymbol{X}_d$, triangle $T$
$(u_{\ell,1}, u_{\ell,2}, u_{\ell,3}) \leftarrow \mathrm{Bar}_T(\boldsymbol{X}_\ell)$, $\ell = 1,2,\dots,d$;
$c_{\boldsymbol{i}}^{(0)} \leftarrow c_{\boldsymbol{i}}$, $\boldsymbol{i} \in \mathbb{I}_d$;
**for** $\ell = 1,2,\dots,d$ **do**
  **foreach** $\boldsymbol{i} \in \mathbb{I}_{d-\ell}$ **do**
    $c_{\boldsymbol{i}}^{(\ell)} \leftarrow u_{\ell,1} c_{\boldsymbol{i}+(1,0,0)}^{(\ell-1)} + u_{\ell,2} c_{\boldsymbol{i}+(0,1,0)}^{(\ell-1)} + u_{\ell,3} c_{\boldsymbol{i}+(0,0,1)}^{(\ell-1)}$;
  **end**
**end**
**Output:** value $c_{(0,0,0)}^{(d)}$

**Remark 2.** In what follows the Algorithm 1 is applied also as

$$\mathtt{DeCast}\big( \boldsymbol{C}, (\boldsymbol{X}_1, \boldsymbol{X}_2, \dots, \boldsymbol{X}_d), T \big) = \mathtt{DeCast}\big( \boldsymbol{C}, (\boldsymbol{u}_1, \boldsymbol{u}_2, \dots, \boldsymbol{u}_d) \big),$$

where $\boldsymbol{u}_\ell = \mathrm{Bar}_T(\boldsymbol{X}_\ell)$, $\ell = 1,2,\dots,d$.

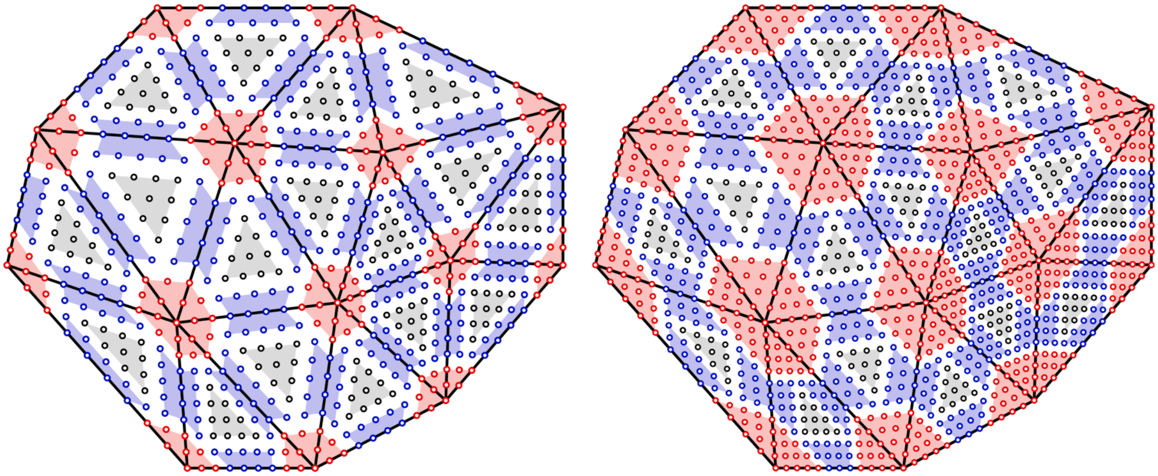

**Fig. 1.** A visual representation of Bézier coefficient groups (red - vertex group, black - triangle group, blue - edge group) for $C^1$ (left) and $C^2$ (right) super-smooth Argyris spline space.

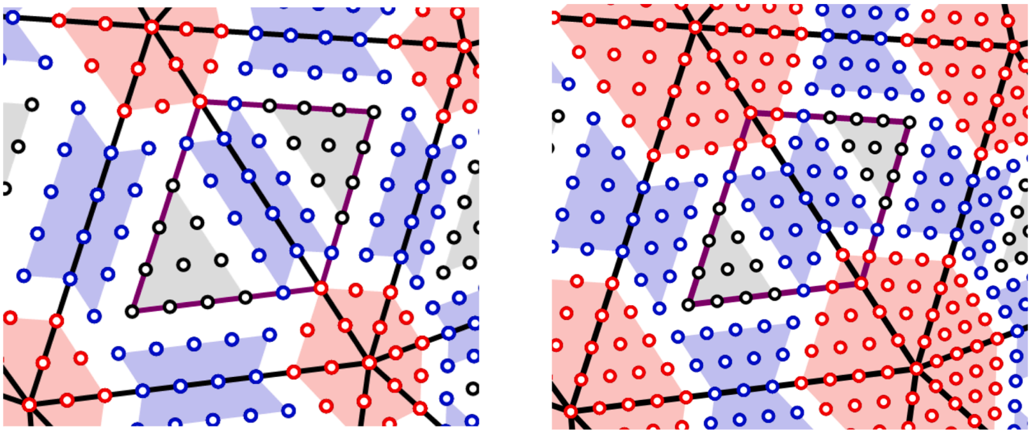

**Fig. 2.** Illustration showing that, due to local support requirements, it is sufficient to study only two adjacent sub-triangles (traced with purple) along a common edge.

### 2.1. A $C^r$ spline space over a triangulation

Let $\Omega \subset \mathbb{R}^2$ be a given planar connected domain with a polygonal boundary partitioned by a triangulation $\Delta = \{T_1, T_2, \ldots, T_M\}$, such that the intersection of two triangles is either empty, a common edge or a vertex, and such that $\Omega = \cup_{m=1}^{M} T_m$. We denote the set of vertices and edges by $\mathcal{V} = \{\boldsymbol{V}_j : j \in \mathcal{I}_\mathcal{V}\}$ and $\mathcal{E} = \{\mathbf{e}_k : k \in \mathcal{I}_\mathcal{E}\}$ respectively, where $\mathcal{I}_\mathcal{V}$ and $\mathcal{I}_\mathcal{E}$ denote the index sets. Observing the spline space

$$\mathcal{S}_d^r(\Delta) := \left\{ s : \Omega \to \mathbb{R} : s|_{T_m} \in \mathbb{P}_d^2, \ m \in \{1, 2, \ldots, M\} \right\} \cap C^r(\Omega)$$

or its subspace, determining the dimension of the space and construction of locally supported non-negative basis functions that form a partition of unity, i.e., B–spline–like basis functions, presents challenging problems.

Due to smoothness conditions that depend on the geometry of the triangles in the triangulation, the coefficients in the Bernstein–Bézier form are usually separated into three groups – *triangle*, *vertex* and *edge* group. Fig. 1 graphically presents this separation for the $C^1$ and $C^2$ super-smooth Argyris spline space, where super-smoothness of order 2 for $C^1$ and order 4 for $C^2$ is imposed at the vertices of a triangulation. Red domain points correspond to *vertex*, black to *triangle*, and blue to *edge* Bézier coefficients. The same separation is applied to basis splines as well (more details are given in Section 3).

As already reviewed in the introduction the construction of vertex basis splines is well developed. It is based on selecting for each vertex of the triangulation the *control triangle*, that contains all the domain points in the vertex group around the chosen vertex. Requiring the $C^s$ continuity at the vertex one chooses over the control triangle the Bernstein basis polynomials of degree $s$ and subdivides them to local triangles (denoted by red in Fig. 1) to determine the values of Bézier coefficients in the vertex group (see [11, Theorem 3]). The *triangle* basis splines are chosen simply as the Bernstein basis polynomials corresponding to domain points in the triangle group extended by zero outside the observed triangle. An approach to compute the non-negative edge basis splines of general degree forming the partition of unity is explored only for $C^1$ continuous splines (see [9]). However, the construction proposed in [9] is done in an algebraic way and does not have a clear geometric interpretation. A novel approach for computing edge basis splines that can be applied to splines of a higher order of smoothness and is based on the selection of specific control triangles is presented in the next section. Due to the requirement of the local support it is sufficient to consider the problem on two triangles sharing an edge as illustrated in Fig. 2 (purple triangles).

## 3. Splines over two triangles sharing an edge

Suppose that the triangulation of a connected domain $\Omega$ consists of only two triangles $\Delta = \{T_1, T_2\}$, $T_1 = (\boldsymbol{S}_1, \boldsymbol{S}_2, \boldsymbol{R}_1)$ and $T_2 = (\boldsymbol{S}_1, \boldsymbol{S}_2, \boldsymbol{R}_2)$, that share the edge $\boldsymbol{e} = (\boldsymbol{S}_1, \boldsymbol{S}_2)$ and form a strictly convex quadrilateral. For a spline $s \in \mathcal{S}_d^r(\Delta)$, $r \geq 0$, we denote its restriction to triangles by

$$s|_{T_\ell} =: p_\ell \in \mathbb{P}_d^2, \quad p_\ell = \sum_{\boldsymbol{i} \in \mathbb{I}_d} c_{\boldsymbol{i}}^{T_\ell} B_{\boldsymbol{i}}^{T_\ell, d}, \quad \ell = 1, 2,$$

where $c^{T_1}_{(d-i,i,0)} = c^{T_2}_{(d-i,i,0)}$, $i = 0, 1, \ldots, d$. To present the Bézier coefficients of $s$ over both triangles we use the following table representation

| | $0$ | $1$ | $\ldots$ | $\ldots$ | $d$ |
|---|---|---|---|---|---|
| $0$ | $c^{T_1}_{(0,0,d)}$ | $0$ | $0$ | $\ldots$ | $0$ |
| $1$ | $c^{T_1}_{(1,0,d-1)}$ | $c^{T_1}_{(0,1,d-1)}$ | $0$ | $\ldots$ | $0$ |
| | $\vdots$ | $\vdots$ | $\ddots$ | $\ddots$ | $\vdots$ |
| $d-1$ | $c^{T_1}_{(d-1,0,1)}$ | $c^{T_1}_{(d-2,1,1)}$ | $\ldots$ | $c^{T_1}_{(0,d-1,1)}$ | $0$ |
| $d$ | $c^{T_1}_{(d,0,0)}$ | $c^{T_1}_{(d-1,1,0)}$ | $\ldots$ | $c^{T_1}_{(1,d-1,0)}$ | $c^{T_1}_{(0,d,0)}$ |
| $d+1$ | $c^{T_2}_{(d-1,0,1)}$ | $c^{T_2}_{(d-2,1,1)}$ | $\ldots$ | $c^{T_2}_{(0,d-1,1)}$ | $0$ |
| | $\vdots$ | $\vdots$ | $\ddots$ | $\ddots$ | $\vdots$ |
| $2d-1$ | $c^{T_2}_{(1,0,d-1)}$ | $c^{T_21}_{(0,1,d-1)}$ | $0$ | $\ldots$ | $0$ |
| $2d$ | $c^{T_2}_{(0,0,d)}$ | $0$ | $0$ | $\ldots$ | $0$ |

(4)

The $C^r$ continuity conditions hold true iff

$$c_{\boldsymbol{i}}^{T_2} = \mathcal{B}[p_1]\left(\boldsymbol{S}_1^{\langle i_1 \rangle}, \boldsymbol{S}_2^{\langle i_2 \rangle}, \boldsymbol{R}_2^{\langle i_3 \rangle}\right), \quad \boldsymbol{i} = (i_1, i_2, i_3) \in \mathbb{I}_d, \quad i_3 \in \{0, 1, \ldots, r\}.$$

Thus, the dimension of this spline space equals $\mathcal{S}_d^r(\Delta) = \binom{d+2}{2} + \binom{d-r+1}{2}$. Let us separate the Bézier coefficients $c_{\boldsymbol{i}}^{T_\ell}$, $\boldsymbol{i} = (i_1, i_2, i_3) \in \mathbb{I}_d$, for $\ell = 1, 2$ into three groups:

- Vertex group: $\mathcal{G}_{\mathcal{V}}^{T_\ell} = \mathcal{G}_{\boldsymbol{S}_1}^{T_\ell} \cup \mathcal{G}_{\boldsymbol{S}_2}^{T_\ell}$, $\mathcal{G}_{\boldsymbol{S}_j}^{T_\ell} := \left\{ c_{\boldsymbol{i}}^{T_\ell} \ : \ d - r + 1 \leq i_j \leq d \right\}$ for $j = 1, 2$,
- Triangle group: $\mathcal{G}_{\triangle}^{T_\ell} = \left\{ c_{\boldsymbol{i}}^{T_\ell} \ : \ r + 1 \leq i_3 \leq d \right\}$,
- Edge group: $\mathcal{G}_{\mathcal{E}}^{T_\ell} = \left\{ c_{\boldsymbol{i}}^{T_\ell} \ : \ 0 \leq i_1 \leq d - r + 2, \ 0 \leq i_2 \leq d - r + 2, \ 0 \leq i_3 \leq r \right\}$,

In Fig. 2 the two observed triangles are denoted in purple and the domain points corresponding to these three groups are colored in red, gray and blue respectively for the $C^1$ (left) and $C^2$ (right) order of smoothness. By denoting

$$n_1 := \left| \mathcal{G}_{\boldsymbol{S}_j}^{T_\ell} \right| = \binom{r+1}{2}, \quad n_2 := \left| \mathcal{G}_{\triangle}^{T_\ell} \right| = \binom{d-r+1}{2}, \quad n_3 := \left| \mathcal{G}_{\mathcal{E}}^{T_\ell} \right| = (d + 1 - 2r)(r + 1) + \binom{r+1}{2}, \tag{5}$$

the dimension can be expressed as $\dim(\mathcal{S}_d^r(\Delta)) = 2n_1 + 2n_2 + n_3$. The goal is to construct $2n_1$, $2n_2$ and $n_3$ B–spline–like basis functions corresponding to the two vertices, two triangles and one edge of $\Delta$, respectively, so that

(a) the *triangle* basis functions have zero Bézier coefficients in the vertex and edge group,
(b) the *edge* basis functions have zero Bézier coefficients in the vertex and triangle group,
(c) the *vertex* basis functions have zero Bézier coefficients in the triangle group,
(d) basis functions are non-negative and form a partition of unity.

Note that, for the *vertex* basis functions, we do not impose the condition that the Bézier coefficients in the edge group are zero, since the smoothness conditions imply that a small number of these coefficients must be non-zero. In what follows, we assume that $d \geq 2r$ ensuring that at least one Bézier coefficient associated with domain points on the common edge appears in the edge group.

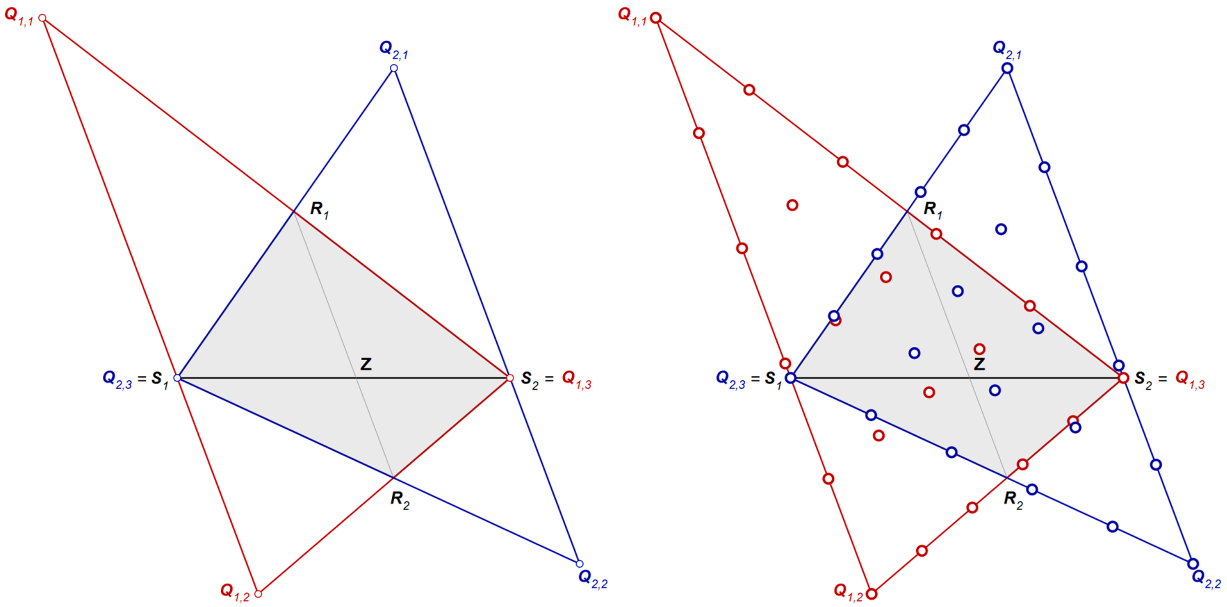


**Fig. 3.** The control triangles $Q_1$ (red) and $Q_2$ (blue) and their domain points for degree $d = 5$.

### 3.1. Control triangles

By assumption, the triangles $T_1$ and $T_2$ form a strictly convex quadrilateral. For the construction of edge B–spline–like basis functions we introduce two so called *control* triangles

$$Q_j = \left(\boldsymbol{Q}_{j,1}, \boldsymbol{Q}_{j,2}, \boldsymbol{Q}_{j,3}\right), \quad j = 1, 2,$$

in the following way (see Fig. 3. Denoting by $\mathrm{line}(\boldsymbol{P}_1, \boldsymbol{P}_2)$ the *line* through points $\boldsymbol{P}_1$ and $\boldsymbol{P}_2$, the vertices of $Q_j$ are chosen as

$$\begin{aligned} \boldsymbol{Q}_{1,1} &= q_1 \cap \mathrm{line}(\boldsymbol{S}_2, \boldsymbol{R}_1), \quad & \boldsymbol{Q}_{1,2} &= q_1 \cap \mathrm{line}(\boldsymbol{S}_2, \boldsymbol{R}_2), \quad & \boldsymbol{Q}_{1,3} &= \boldsymbol{S}_2, \\ \boldsymbol{Q}_{2,1} &= q_2 \cap \mathrm{line}(\boldsymbol{S}_1, \boldsymbol{R}_1), \quad & \boldsymbol{Q}_{2,2} &= q_2 \cap \mathrm{line}(\boldsymbol{S}_1, \boldsymbol{R}_2), \quad & \boldsymbol{Q}_{2,3} &= \boldsymbol{S}_1, \end{aligned}$$

where $q_j = \mathrm{line}(\boldsymbol{S}_j, \boldsymbol{S}_j + \boldsymbol{R}_1 - \boldsymbol{R}_2)$ is the line through $\boldsymbol{S}_j$ parallel to the $\mathrm{line}(\boldsymbol{R}_1, \boldsymbol{R}_2)$.

Further, let the barycentric coordinates of $\boldsymbol{R}_2$ with respect to $T_1$ be denoted by $\mathrm{Bar}_{T_1}(\boldsymbol{R}_2) =: (\sigma_1, \sigma_2, \rho)$, and let $\boldsymbol{Z}$ be the intersection between $\mathrm{line}(\boldsymbol{R}_1, \boldsymbol{R}_2)$ and $\mathrm{line}(\boldsymbol{S}_1, \boldsymbol{S}_2)$. It is straightforward to compute that

$$\boldsymbol{Z} = \mu_1 \boldsymbol{R}_1 + \mu_2 \boldsymbol{R}_2 = \lambda_1 \boldsymbol{S}_1 + \lambda_2 \boldsymbol{S}_2, \quad \mu_1 := \tfrac{-\rho}{1-\rho}, \quad \mu_2 := \tfrac{1}{1-\rho}, \quad \lambda_1 := \tfrac{\sigma_1}{\sigma_1+\sigma_2}, \quad \lambda_2 := \tfrac{\sigma_2}{\sigma_1+\sigma_2}. \tag{6}$$

Note that $\rho < 0$ and $\sigma_j, \mu_j, \lambda_j > 0$ for $j = 1, 2$, since the triangles are assumed to form a strictly convex quadrilateral. Moreover, it is straightforward to compute that

$$\begin{aligned} &\mathrm{Bar}_{Q_1}(\boldsymbol{S}_1) = \left(\mu_1, \mu_2, 0\right), \quad \mathrm{Bar}_{Q_1}(\boldsymbol{S}_2) = (0, 0, 1), \quad \mathrm{Bar}_{Q_1}(\boldsymbol{R}_1) = \left(\lambda_1, 0, \lambda_2\right), \quad \mathrm{Bar}_{Q_1}(\boldsymbol{R}_2) = \left(0, \lambda_1, \lambda_2\right) \\ &\mathrm{Bar}_{Q_2}(\boldsymbol{S}_1) = (0, 0, 1), \quad \mathrm{Bar}_{Q_2}(\boldsymbol{S}_2) = \left(\mu_1, \mu_2, 0\right), \quad \mathrm{Bar}_{Q_2}(\boldsymbol{R}_1) = \left(\lambda_2, 0, \lambda_1\right), \quad \mathrm{Bar}_{Q_2}(\boldsymbol{R}_2) = \left(0, \lambda_2, \lambda_1\right), \end{aligned}$$

and the areas of control triangles satisfy

$$\mathrm{area}(Q_j) = \frac{\mathrm{area}(T_1) + \mathrm{area}(T_2)}{\lambda_j}, \quad j = 1, 2. \tag{7}$$

Over $Q_j$ for $j = 1, 2$, we choose $\binom{d+2}{2}$ Bernstein basis polynomials $B_{\boldsymbol{k}}^{Q_j,d}$, $\boldsymbol{k} = (k_1, k_2, k_3) \in \mathbb{I}_d$, that clearly lie in $\mathcal{S}_d^r(\Delta)$. Their schematic representation for $d = 5$ is shown in Fig. 3 (right), where each red dot represents one Bernstein basis polynomial over $Q_1$, and the blue dot the Bernstein basis polynomial over $Q_2$. Their Bernstein–Bézier representation over $\Delta$, obtained by the subdivision onto $T_1$ and $T_2$, is given in the following theorem.

**Theorem 1.** *Let*

$$B_{\boldsymbol{k}}^{Q_j,d}\Big|_{T_\ell} = \sum_{\boldsymbol{i} \in \mathbb{I}_d} b[\boldsymbol{k}, Q_j, T_\ell]_{\boldsymbol{i}} B_{\boldsymbol{i}}^{T_\ell,d}, \quad j = 1, 2, \quad \ell = 1, 2, \quad \boldsymbol{k} \in \mathbb{I}_d.$$

*The Bézier coefficients are equal to*

$$b[\boldsymbol{k}, Q_1, T_1]_{\boldsymbol{i}} = \begin{cases} B_{i_1-k_2}^{i_1}(\mu_1) B_{k_1+k_2-i_1}^{i_3}(\lambda_1), & (k_2 \le i_1 \le k_1 + k_2) \wedge (i_2 \le k_3) \\ 0, & \text{elsewise} \end{cases}, \tag{8a}$$

$$b[\boldsymbol{k},Q_1,T_2]_{\boldsymbol{i}} = \begin{cases} B^{i_1}_{k_1}(\mu_1)B^{i_3}_{k_1+k_2-i_1}(\lambda_1), & (k_1 \le i_1 \le k_1+k_2) \wedge (i_2 \le k_3) \\ 0, & \text{elsewise} \end{cases}, \tag{8b}$$

$$b[\boldsymbol{k},Q_2,T_1]_{\boldsymbol{i}} = \begin{cases} B^{i_2}_{i_2-k_2}(\mu_1)B^{i_3}_{k_3-i_1}(\lambda_1), & (k_2 \le i_2 \le k_1+k_2) \wedge (i_1 \le k_3) \\ 0, & \text{elsewise} \end{cases}, \tag{8c}$$

$$b[\boldsymbol{k},Q_2,T_2]_{\boldsymbol{i}} = \begin{cases} B^{i_2}_{k_1}(\mu_1)B^{i_3}_{k_3-i_1}(\lambda_1), & (k_1 \le i_2 \le k_1+k_2) \wedge (i_1 \le k_3) \\ 0, & \text{elsewise} \end{cases}. \tag{8d}$$

**Proof.** We denote by $I_{\boldsymbol{k},d} \in \mathbb{R}^{(d+1)\times(d+1)}$ the matrix with $I_{\boldsymbol{k},d}(d-k_3,k_2) = 1$ and zero values elsewhere. Assume first that $j=1$. By (3) the Bézier coefficients of $B^{Q_1,d}_{\boldsymbol{k}}$ observed over $T_1$ are for all $\boldsymbol{i} = (i_1,i_2,i_3) \in \mathbb{I}_d$ equal to

$$\begin{aligned} b[\boldsymbol{k},Q_1,T_1]_{\boldsymbol{i}} &= \mathcal{B}[B^{Q_1,d}_{\boldsymbol{k}}]\left(\boldsymbol{S}_1^{\langle i_1\rangle}, \boldsymbol{S}_2^{\langle i_2\rangle}, \boldsymbol{R}_1^{\langle i_3\rangle}\right) = \mathtt{DeCast}\left(I_{\boldsymbol{k},d}, \left(\boldsymbol{S}_1^{\langle i_1\rangle}, \boldsymbol{S}_2^{\langle i_2\rangle}, \boldsymbol{R}_1^{\langle i_3\rangle}\right), \boldsymbol{T}\right) \\ &= \mathtt{DeCast}\left(I_{\boldsymbol{k},d}, \left((\mu_1,\mu_2,0)^{\langle i_1\rangle}, (0,0,1)^{\langle i_2\rangle}, (\lambda_1,0,\lambda_2)^{\langle i_3\rangle}\right)\right) \\ &= \mathtt{DeCast}\left(I_{(k_1,k_2,k_3-i_2),d-i_2}, \left((\mu_1,\mu_2,0)^{\langle i_1\rangle}, (\lambda_1,0,\lambda_2)^{\langle i_3\rangle}\right)\right), \end{aligned}$$

where the last equality follows by applying $i_2$–times the argument $(0,0,1)$. From well known properties of the de Casteljau algorithm, we further derive that

$$b[\boldsymbol{k},Q_1,T_1]_{\boldsymbol{i}} = \sum_{\boldsymbol{j}\in\mathbb{I}_{i_3}} \left( \sum_{\boldsymbol{s}\in\mathbb{I}_{i_1}} c_{\boldsymbol{j}+\boldsymbol{s}+(0,0,i_2)} B^{\triangle,i_1}_{\boldsymbol{s}}(\mu_1,\mu_2,0) \right) B^{\triangle,i_3}_{\boldsymbol{j}}(\lambda_1,0,\lambda_2),$$

where $c_{\boldsymbol{k}} = 1$ and $c_{\boldsymbol{\ell}} = 0$ for all $\boldsymbol{\ell} \ne \boldsymbol{k}$. Since

$$B^{\triangle,i_1}_{(s_1,s_2,s_3)}(\mu_1,\mu_2,0) = \begin{cases} B^{i_1}_{s_1}(\mu_1), & s_3 = 0 \\ 0, & \text{elsewise} \end{cases}, \quad B^{\triangle,i_3}_{(j_1,j_2,j_3)}(\lambda_1,0,\lambda_2) = \begin{cases} B^{i_3}_{j_1}(\lambda_1), & j_2 = 0 \\ 0, & \text{elsewise} \end{cases},$$

it follows that

$$b[\boldsymbol{k},Q_1,T_1]_{\boldsymbol{i}} = \sum_{j_1=0}^{i_3} \sum_{s_1=0}^{i_1} c_{(j_1+s_1,i_1-s_1,i_3-j_1+i_2)} B^{i_1}_{s_1}(\mu_1) B^{i_3}_{j_1}(\lambda_1),$$

which by assuming that only $c_{\boldsymbol{k}}$ is nonzero implies (8a). Similarly we derive (8b)–(8d). This completes the proof. □

### 3.2. *Candidates for B–spline–like basis functions*

Theorem 1 reveals that many of the coefficients $b[\boldsymbol{k},Q_j,T_\ell]_{\boldsymbol{s}}$, $\boldsymbol{s} = (s_1,s_2,s_3) \in \mathbb{I}_d$, are equal to zero. Graphical illustration and the schematic table representation (4) of nonzero Bézier coefficients of $B^{Q_j,d}_{\boldsymbol{k}}$ for $\boldsymbol{k} = (i, d-k-i, k)$, $i = 0,1,\dots,d-k$ for a fixed $k = k_3$, and $j = 1$ are shown in Fig. 4. Similar illustration for $j = 2$ is provided in Fig. 5. Circled domain points denote which Bernstein basis polynomial is used, and black domain points (and blue fields in table representation) indicate nonzero coefficients after the subdivision.

Since the Bézier coefficients $b[\boldsymbol{k},Q_j,T_\ell]_{\boldsymbol{s}}$ with $s_3 > r$ do not affect the $C^r$ smoothness conditions, the splines obtained from $B^{Q_j,d}_{\boldsymbol{k}}$ by setting these coefficients over both triangles $T_1$ and $T_2$ to zero remain in $\mathcal{S}^r_d(\Delta)$. Let us denote these splines by $\widetilde{B}^{Q_j,d}_{\boldsymbol{k}}$. Note that they are not linearly independent anymore. In more detail, for a fixed $k = k_3$ and the control triangle $Q_1$, we have $d-k+1$ splines $\widetilde{B}^{Q_1,d}_{(i,d-k-i,k)}$, $i = 0,1,\dots,d-k$. Each can be represented with a matrix of Bézier coefficients over $T_1$ and a matrix over $T_2$, joined in a table of the form (4). As illustrated in Fig. 4 and certified by Theorem 1, all Bézier coefficients of the spline $\widetilde{B}^{Q_1,d}_{(i,d-k-i,k)}$ in columns indexed from $k+1$ to $d$ vanish. This implies that splines obtained from different levels regarding the index $k$ are linearly independent. Similarly, for the control triangle $Q_2$, fixed $k$ and $\boldsymbol{k} = (i, k-i, d-k)$, $i = 0,1,\dots,k$, we have $k+1$ splines $\widetilde{B}^{Q_2,d}_{(i,k-i,d-k)}$, that also have zero Bézier coefficients in columns indexed from $k+1$ to $d$ (see Fig. 5).

The following lemma shows that the number of linearly independent splines for a fixed $k$ and a fixed control triangle $Q_j$ is at most $r+1$.

**Lemma 1.** (a) *Let $k \in \{0,1,\dots,d-r\}$ be fixed. The set $\left\{ \widetilde{B}^{Q_1,d}_{(i,d-k-i,k)},\ i = 0,1,\dots,d-k \right\}$ contains exactly $r+1$ linearly independent splines.*

(b) *For a fixed $k \in \{d-r+1,\dots,d\}$, all splines in $\left\{ \widetilde{B}^{Q_1,d}_{(i,d-k-i,k)},\ i = 0,1,\dots,d-k \right\}$ are linearly independent.*

(c) *Let $k \in \{r, r+1,\dots,d\}$ be fixed. The set $\left\{ \widetilde{B}^{Q_2,d}_{(i,k-i,d-k)},\ i = 0,1,\dots,k \right\}$ contains exactly $r+1$ linearly independent splines.*

(d) *For a fixed $k \in \{0,1,\dots,r-1\}$, all splines in $\left\{ \widetilde{B}^{Q_2,d}_{(i,k-i,d-k)},\ i = 0,1,\dots,k \right\}$ are linearly independent.*

**Proof.** It suffices to prove statements (a) and (b), since (c) and (d) can be proved in a similar manner.

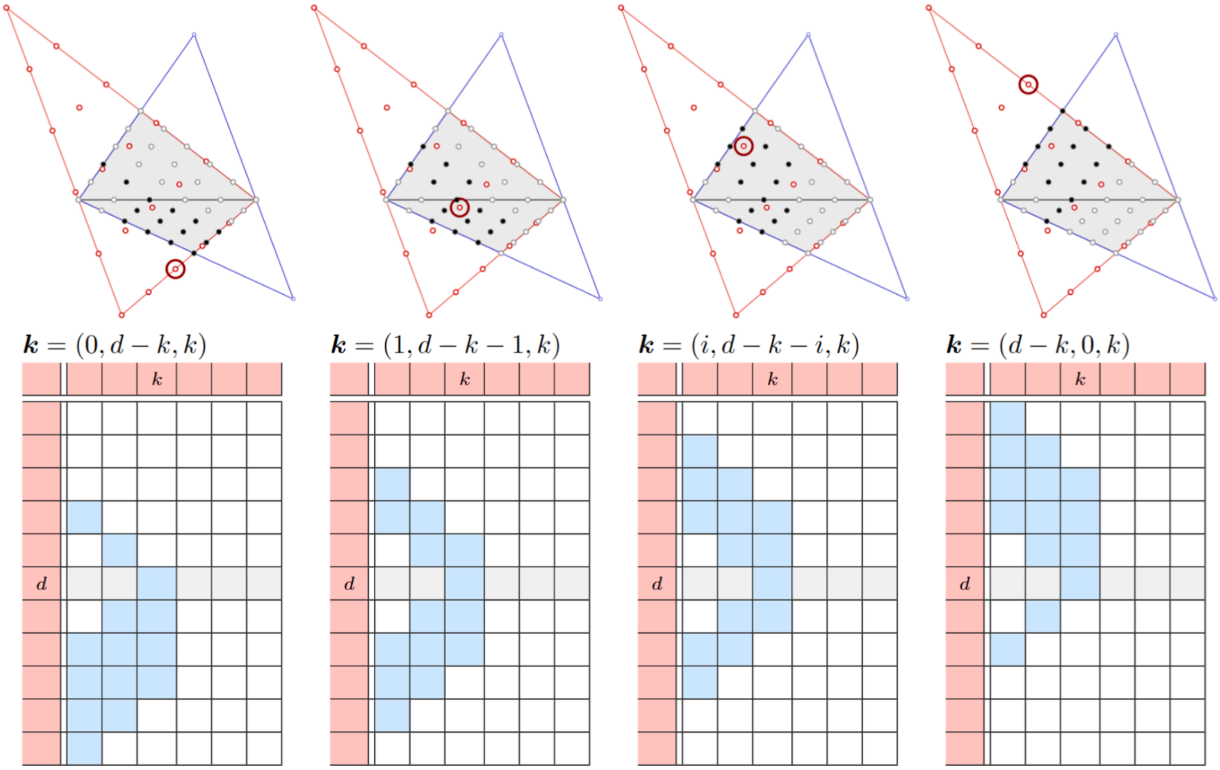


**Fig. 4.** The top row of plots shows the nonzero coefficients over $T_1$ and $T_2$ (colored black) corresponding to the Bernstein polynomial over $Q_1$ associated with the chosen domain point (circled in red) for $d = 5$ and $k = 2$. The corresponding coefficient tables are shown below, with nonzero entries shaded in blue.

**Proof of** (a): To examine linear independence, let us observe a linear combination $\sum_{i=0}^{d-k} \zeta_i \, \widetilde{B}^{Q_1,d}_{(i,d-k-i,k)}$ for $\zeta_i \in \mathbb{R}$. It is zero iff the Bézier coefficients in its Bernstein–Bézier form are all zero. It is enough to consider only the triangle $T_1$ and the coefficients with indices $\boldsymbol{s} = (s_1, s_2, s_3) \in \mathbb{I}_d$ for $s_3 \le r$, which gives the following equations for $(\zeta_i)_{i=0}^{d-k}$:

$$\sum_{i=0}^{d-k} \zeta_i \, b[(i, d-k-i, k), Q_1, T_1]_{\boldsymbol{s}} = 0, \quad \boldsymbol{s} = (s_1, s_2, s_3) \in \mathbb{I}_d, \quad s_3 \le r.$$

By (8a), the spline $\widetilde{B}^{Q_1,d}_{(i,d-k-i,k)}$ has non-zero Bézier coefficients over $T_1$ only at indices $(s_1, s_2, s_3)$ satisfying $d-k-i \le s_1 \le d-k$, $s_2 \le k$, $s_3 \le r$. Since $s_1 = d - s_2 - s_3$, the last two bounds imply that $s_1 \ge d-k-r$. The nontrivial equations are thus, by applying (8a), equal to

$$B^{s_3}_{d-k-s_1}(\lambda_1) \sum_{i=d-k-s_1}^{d-k} \zeta_i \, B^{s_1}_{s_1-(d-k-i)}(\mu_1) = 0, \quad s_1 = d-k-r, \ldots, d-k, \quad s_3 = 0, 1, \ldots, r,$$

showing that for a fixed $s_1$ all the equations are the same. Thus not more than $r+1$ splines can be linearly independent. It is straightforward to see that the first $r+1$ splines, corresponding to $i = 0, 1, \ldots, r$, are linearly independent as each of these splines progressively adds a new non-zero Bézier coefficient over $T_1$ in the $k$-th column of the matrix representation (see Fig. 4 for the illustration). Similarly, by observing non-zero Bézier coefficients over $T_2$ in the $k$-th column, one can see that the last $r+1$ splines, corresponding to $i = d-k-r, \ldots, d-k$, are linearly independent as well.

**Proof of** (b): For $k > d-r$ the set of splines in case (b) of the lemma contains fewer than $r+1$ functions. Their linear independence is immediate, since each spline progressively adds a new non-zero Bézier coefficient over $T_1$ in the $k$-th column of the matrix representation. □

Based on the above observations, results given by Lemma 1 (and its proof), and the aim to preserve the partition of unity property, we propose to join the splines $\widetilde{B}^{Q_j,d}_{\boldsymbol{k}}$ with respect to $k_3 = k$ in the following way:

$$k \in \{0, \ldots, r-1\} : \varphi^{Q_1}_{k,i+1} = \widetilde{B}^{Q_1,d}_{(i,d-k-i,k)}, \;\; \varphi^{Q_2}_{d-k,k+1-i} = \widetilde{B}^{Q_2,d}_{(i,d-k-i,k)}, \;\; i = 0, 1, \ldots, k-1, \tag{9a}$$

$$\varphi^{Q_1}_{k,k+1} = \sum_{i=k}^{d-k} \widetilde{B}^{Q_1,d}_{(i,d-k-i,k)}, \quad \varphi^{Q_2}_{d-k,1} = \sum_{i=k}^{d-k} \widetilde{B}^{Q_2,d}_{(i,d-k-i,k)} \tag{9b}$$

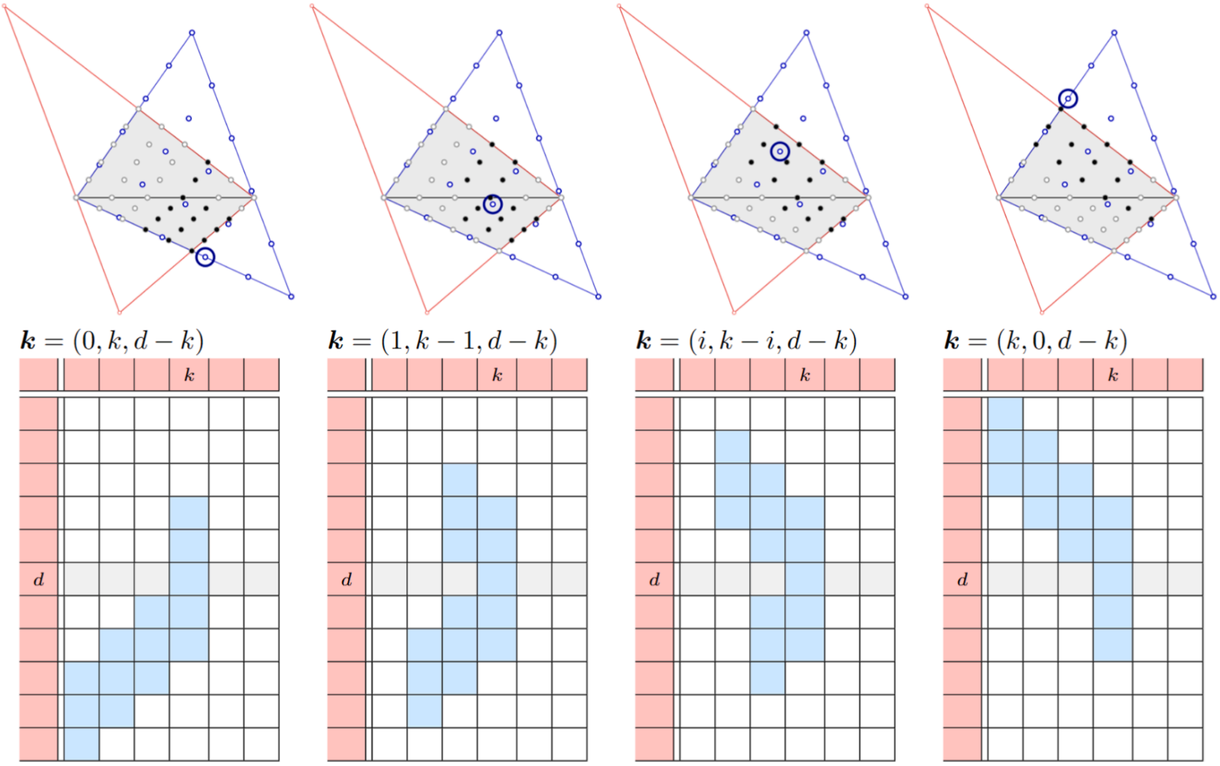


**Fig. 5.** The top row of plots shows the nonzero coefficients over $T_1$ and $T_2$ (colored black) corresponding to the Bernstein polynomial over $Q_2$ associated with the chosen domain point (circled in blue) for $d = 5$ and $d - k = 2$. The corresponding coefficient tables are shown below, with nonzero entries shaded in blue.

$$k \in \{r, \dots, d-r\} : \varphi^{Q_1}_{k,i+1} = \widetilde{B}^{Q_1,d}_{(i,d-k-i,k)}, \ \varphi^{Q_2}_{d-k,r+1-i} = \widetilde{B}^{Q_2,d}_{(i,d-k-i,k)}, \ i = 0, 1, \dots, r-1, \tag{9c}$$

$$\varphi^{Q_1}_{k,r+1} = \sum_{i=r}^{d-k} \widetilde{B}^{Q_1,d}_{(i,d-k-i,k)}, \quad \varphi^{Q_2}_{d-k,1} = \sum_{i=r}^{d-k} \widetilde{B}^{Q_2,d}_{(i,d-k-i,k)} \tag{9d}$$

$$k \in \{d-r+1, \dots, d\} : \varphi^{Q_1}_{k,i+1} = \widetilde{B}^{Q_1,d}_{(i,d-k-i,k)}, \ \varphi^{Q_2}_{d-k,d-k+1-i} = \widetilde{B}^{Q_2,d}_{(i,d-k-i,k)}, \ i = 0, 1, \dots, d-k. \tag{9e}$$

The coupling (9) is graphically illustrated for $C^1$ and $C^2$ splines of degree $d = 5$ in Figs. 6 and 7, respectively.

For a fixed $j \in \{1, 2\}$, the splines defined in (9) are linearly independent and their sum has in its Bernstein–Bézier representation all the coefficients in the vertex and edge group equal to one. For $0 \le k \le r-1$ and $d-r+1 \le k \le d$ definition (9) yields $2\binom{r+1}{2}$ spline functions that belong to a group of vertex basis functions. Thus only one of $Q_1$ or $Q_2$ would be needed to derive the vertex basis functions. Furthermore, for a fixed $j \in \{1, 2\}$ and $r \le k \le d-r$ we obtain $(d+1-2r)(r+1)$ functions that belong to a group of edge spline functions, since their Bézier coefficients in $\mathcal{G}^{T_\ell}_{\mathcal{V}}$ are all equal to zero. Recalling (5) (and applying the result of Lemma 1), we observe that using only a single control triangle does not provide a sufficient number of edge basis functions, as it gives $\binom{r+1}{2}$ too few splines. For this reason, we need to combine the splines obtained from both control triangles $Q_1$ or $Q_2$ in order to obtain $n_3$ linearly independent splines and with the aim to keep the partition of unity property, inherited from the Bernstein basis polynomials $B^{Q_j,d}_{\boldsymbol{k}}$. In the next two sections we study in detail the $C^1$ and $C^2$ case.

**Remark 3.** Note that the definition of the functions in (9) depends on the ordering of triangles $T_1$ and $T_2$. Specifically, for a fixed $k$, we select individually the Bernstein basis polynomials corresponding to the "bottom" few domain points (closer to $\boldsymbol{R}_2$), and we sum the ones above (see Fig. 6 and Fig. 7). Interchanging the roles of $T_1$ and $T_2$, that is, exchanging $\boldsymbol{R}_1$ and $\boldsymbol{R}_2$, is equivalent to selecting individually the Bernstein basis polynomials corresponding to the "top" few domain points individually and summing those below.

**Remark 4.** It would also be natural to consider couplings in which the grouping associated with one control triangle is reversed with respect to that of the other. In particular, changing the order of vertices in the control triangle $Q_1 = (\boldsymbol{Q}_{1,1}, \boldsymbol{Q}_{1,2}, \boldsymbol{Q}_{1,3})$ to $(\boldsymbol{Q}_{1,2}, \boldsymbol{Q}_{1,1}, \boldsymbol{Q}_{1,3})$ while keeping $Q_2$ unchanged, yields the configuration in which the grouping associated with $Q_1$ is reversed with respect to that of $Q_2$, i.e., the Bernstein basis polynomials corresponding to the "top" few domain points are selected individually, while those below are summed together. The analysis of such a configuration would require a separate treatment. Since numerical experiments showed (see also Example 1) that, with respect to the criteria introduced in the next section, this choice (as well as the

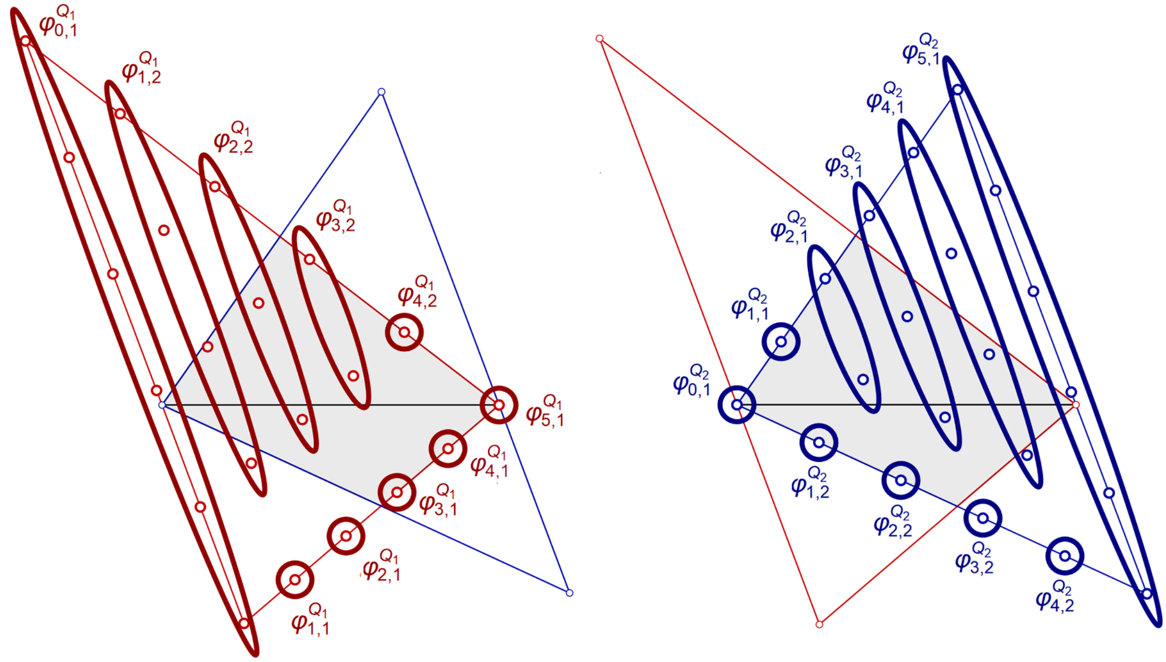


**Fig. 6.** A graphical illustration of the coupling (9) for $C^1$ splines of degree $d = 5$: all the Bernstein basis polynomials over $Q_1$ (left) or $Q_2$ (right) corresponding to domain points circled in red or blue are summed together.

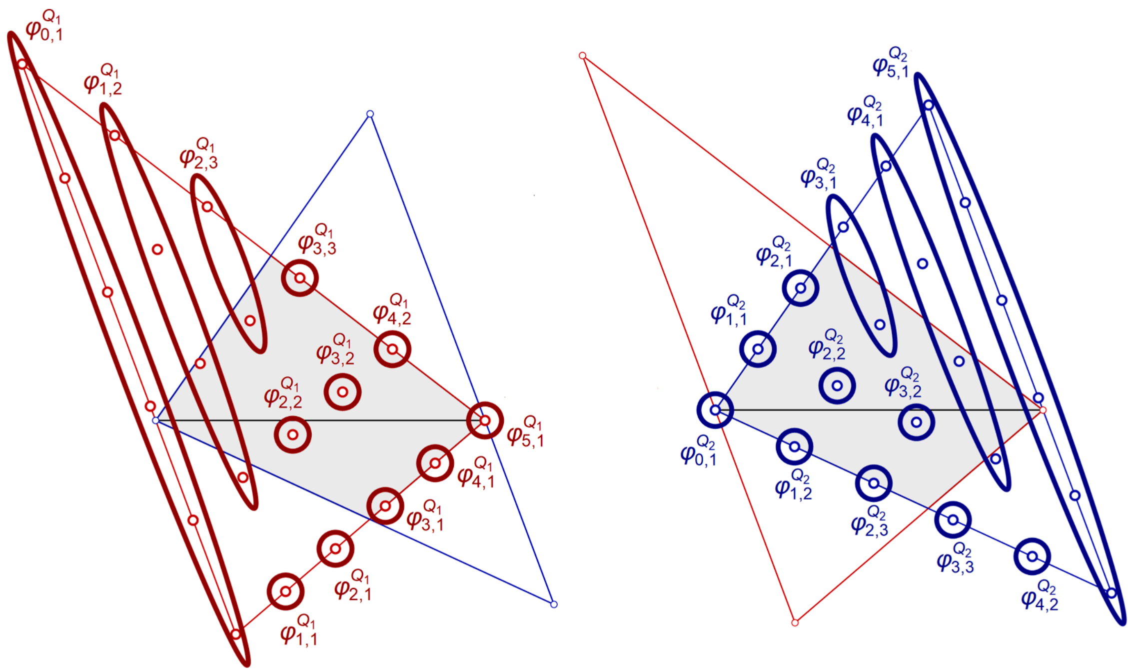


**Fig. 7.** A graphical illustration of the coupling (9) for $C^2$ splines of degree $d = 5$: all the Bernstein basis polynomials over $Q_1$ (left) or $Q_2$ (right) corresponding to domain points circled in red or blue are summed together.

choice obtained by exchanging the roles of $Q_1$ and $Q_2$) does not lead to bases exhibiting better properties than the bases presented in the remainder of the paper, we omit the corresponding analysis.

## 4. $C^1$ Continuous B–spline–like basis functions

For $r = 1$ the spline functions defined in (9) have non-zero Bézier coefficients, presented in the table representation (4), only in rows $d-1$, $d$ and $d+1$. Namely, the non-zero coefficients in these rows are equal to

$\varphi_{0,1}^{Q_1} = \varphi_{0,1}^{Q_2}$ :

| 0 | 1 | | $k-1$ | $k$ | | | $d$ |
|---|---|---|---|---|---|---|---|
| $\lambda_1$ | | | | | | | |
| 1 | | | | | | | |
| $\lambda_1$ | | | | | | | |

, $\varphi_{d,1}^{Q_1} = \varphi_{d,1}^{Q_2}$ :

| 0 | 1 | | $k-1$ | $k$ | | | $d$ |
|---|---|---|---|---|---|---|---|
| | | | | | | $\lambda_2$ | |
| | | | | | | | 1 |
| | | | | | | $\lambda_2$ | |

, (10a)

and

$\varphi_{k,1}^{Q_1}$ :

| 0 | 1 | | $k-1$ | $k$ | | | $d$ |
|---|---|---|---|---|---|---|---|
| | | | $\lambda_2\mu_2^{d-k}$ | 0 | | | |
| | | | 0 | $\mu_2^{d-k}$ | | | |
| | | | $\lambda_2\mu_2^{d-k}$ | $\lambda_1\mu_2^{d-k-1}$ | | | |

, $\varphi_{k,1}^{Q_2}$ :

| 0 | 1 | | $k-1$ | $k$ | | | $d$ |
|---|---|---|---|---|---|---|---|
| | | | $\lambda_2$ | $\lambda_1(1-\mu_2^k)$ | | | |
| | | | 0 | $1-\mu_2^k$ | | | |
| | | | $\lambda_2(1-\mu_2^{k-1})$ | $\lambda_1(1-\mu_2^k)$ | | | |

,

$\varphi_{k,2}^{Q_1}$ :

| 0 | 1 | | $k-1$ | $k$ | | | $d$ |
|---|---|---|---|---|---|---|---|
| | | | $\lambda_2(1-\mu_2^{d-k})$ | $\lambda_1$ | | | |
| | | | 0 | $1-\mu_2^{d-k}$ | | | |
| | | | $\lambda_2(1-\mu_2^{d-k})$ | $\lambda_1(1-\mu_2^{d-k-1})$ | | | |

, $\varphi_{k,2}^{Q_2}$ :

| 0 | 1 | | $k-1$ | $k$ | | | $d$ |
|---|---|---|---|---|---|---|---|
| | | | 0 | $\lambda_1\mu_2^k$ | | | |
| | | | 0 | $\mu_2^k$ | | | |
| | | | $\lambda_2\mu_2^{k-1}$ | $\lambda_1\mu_2^k$ | | | |

(10b)

for $k = 1, 2, \ldots, d-1$. We collect these spline functions from each control triangle $Q_j$, $j = 1, 2$ into the ordered set

$$\boldsymbol{\varphi}^{Q_j} := \left\{ \varphi_{0,1}^{Q_j} \right\} \cup \left\{ \varphi_{k,1}^{Q_j}, \varphi_{k,2}^{Q_j} : \ k = 1, 2, \ldots, d-1 \right\} \cup \left\{ \varphi_{d,1}^{Q_j} \right\},$$

where the first and the last spline functions give the vertex basis splines

$$E_0 := \varphi_{0,1}^{Q_1} = \varphi_{0,1}^{Q_2}, \quad E_{2d} := \varphi_{d,1}^{Q_1} = \varphi_{d,1}^{Q_2}, \tag{11a}$$

while for the edge basis splines, in order to obtain the required number of functions, we propose to combine splines from $\boldsymbol{\varphi}^{Q_1}$ and $\boldsymbol{\varphi}^{Q_2}$ as

$$E_1 = \xi_2 \varphi_{1,1}^{Q_2}, \quad E_2 = \xi_1 \varphi_{1,1}^{Q_1} + \xi_2 \varphi_{1,2}^{Q_2}, \quad E_3 = \xi_1 \varphi_{1,2}^{Q_1} \tag{11b}$$

for $d = 2$, and

$$\begin{aligned}
&E_{2i-1} = \varphi_{i,1}^{Q_2}, \quad E_{2i} = \varphi_{i,2}^{Q_2}, \quad i = 1, 2, \ldots, \ell_1, \\
&E_{2\ell_1+1} = \xi_2 \varphi_{\ell_1+1,1}^{Q_2}, \\
&E_{2i} = \xi_1 \varphi_{i,1}^{Q_1} + \xi_2 \varphi_{i,2}^{Q_2}, \quad E_{2i+1} = \xi_1 \varphi_{i,2}^{Q_1} + \xi_2 \varphi_{i+1,1}^{Q_2}, \quad i = \ell_1 + 1, \ldots, d - \ell_2 - 2, \\
&E_{2(d-\ell_2-1)} = \xi_1 \varphi_{d-\ell_2-1,1}^{Q_1} + \xi_2 \varphi_{d-\ell_2-1,2}^{Q_2}, \\
&E_{2(d-\ell_2-1)+1} = \xi_1 \varphi_{d-\ell_2-1,2}^{Q_1}, \\
&E_{2i} = \varphi_{i,1}^{Q_1}, \quad E_{2i+1} = \varphi_{i,2}^{Q_1}, \quad i = d - \ell_2, \ldots, d-1,
\end{aligned} \tag{11c}$$

for $d \geq 3$, where

$$\text{(a) } \ell_1 = \left\lceil \tfrac{d-3}{2} \right\rceil, \ \ell_2 = d - 3 - \ell_1, \quad \text{(b) } \ell_1 = \left\lfloor \tfrac{d-3}{2} \right\rfloor, \ \ell_2 = d - 3 - \ell_2, \tag{12}$$

and $\xi_1, \xi_2 \in (0, 1)$, $\xi_1 + \xi_2 = 1$, are any two chosen parameters. Note that for odd degree $d$ both choices are the same, while for even degree $d \geq 4$ the choice (a) takes more functions from $Q_2$ and (b) takes more from $Q_1$. A graphical illustration of this proposed coupling for $2 \leq d \leq 5$ is shown in Fig. 8. Black border quadrilaterals indicate the selected vertex basis functions. Green border quadrilaterals represent splines that are individually included in the edge group, while green connecting lines signify that a convex combination of two splines is included in the edge group. Thin green border quadrilaterals denote that each function in the first row is multiplied by $\xi_1$ and each function in the second row by $\xi_2$.

The next theorem provides the main result of this section. By the *partition of unity property*, we mean that the sum of all the splines has in its Bernstein–Bézier representation all the coefficients in the vertex and edge group equal to one.

**Theorem 2.** *Let $d \geq 2$ and let $\xi_1, \xi_2 \in (0, 1)$, $\xi_1 + \xi_2 = 1$, be any two chosen values. The splines $E_i$, $i = 0, 1, \ldots, 2d$, given by (11), are for both choices (12) linearly independent, satisfy the partition of unity property, and are non-negative over $T_1 \cup T_2$.*

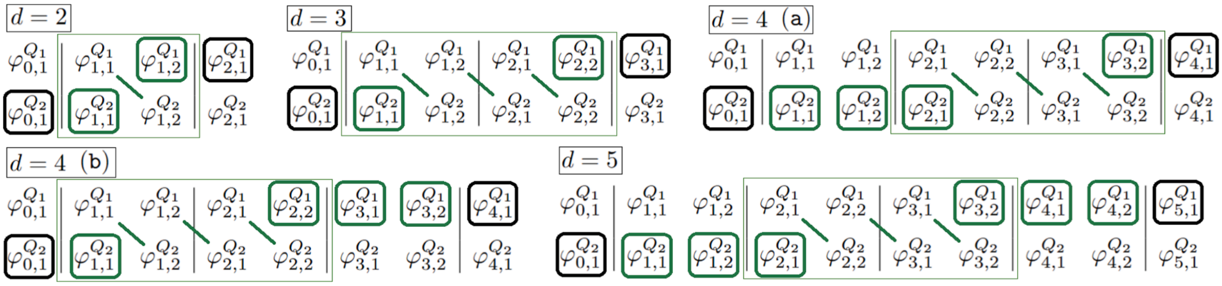


**Fig. 8.** A graphical illustration of the 2nd coupling for $C^1$ with varying degrees $d$. The first $2\ell_1+1$ splines are taken from $Q_2$, the last $2\ell_2+1$ from $Q_1$ and the middle ones are scaled and (possibly) combined as indicated by the diagonal lines.

To prove the theorem, we first introduce the coefficient ordering for the representation of Bézier coefficients (with $i_3 \le 1$) of splines in $\boldsymbol{\varphi}^{Q_j}$, restricted to the triangle $T_1$ or $T_2$:

$$\boldsymbol{c} = (c_{(d,0,0)}, c_{(d-1,0,1)}, c_{(d-1,1,0)}, c_{(d-2,1,1)}, \dots, c_{(1,d-1,0)}, c_{(0,d-1,1)}, c_{(0,d,0)})^T. \tag{13}$$

Since the Bézier coefficients with $i_3 \le 1$ over $T_1$ are uniquely determined by those over $T_2$ via the $C^1$ continuity conditions, and vice versa, we restrict the analysis to the triangle $T_1$. The following lemma which follows directly from (10) is further needed.

**Lemma 2.** *Let $\boldsymbol{C}^{Q_j}$ denote the $(2d+1)\times 2d$ matrix with values of Bézier coefficients (13) (corresponding to rows) which belong to splines (corresponding to columns) in the ordered set $\boldsymbol{\varphi}^{Q_j}$ restricted to $T_1$. The two matrices are equal to*

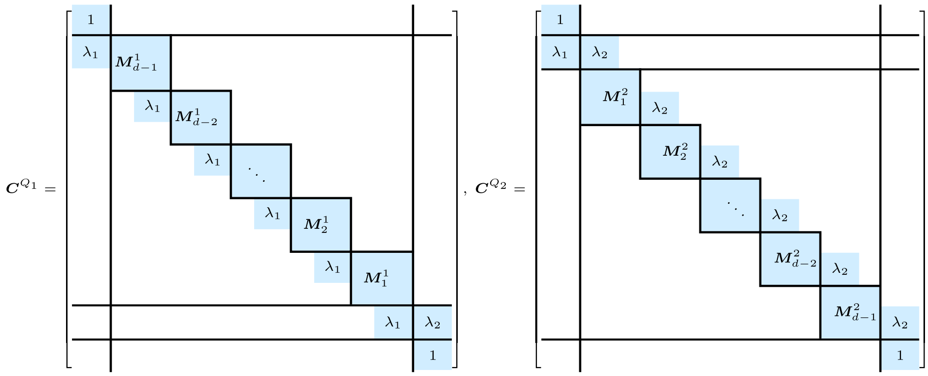


*where*

$$\boldsymbol{M}_k^1 = \begin{bmatrix} \lambda_2 \\ 1 \end{bmatrix} \cdot \begin{bmatrix} \mu_2^k & 1-\mu_2^k \end{bmatrix} = \begin{bmatrix} \lambda_2\mu_2^k & \lambda_2(1-\mu_2^k) \\ \mu_2^k & (1-\mu_2^k) \end{bmatrix}, \quad k = 1,2,\dots,d-1,$$

*and*

$$\boldsymbol{M}_k^2 = \begin{bmatrix} 1 \\ \lambda_1 \end{bmatrix} \cdot \begin{bmatrix} 1-\mu_2^k & \mu_2^k \end{bmatrix} = \begin{bmatrix} (1-\mu_2^k) & \mu_2^k \\ \lambda_1(1-\mu_2^k) & \lambda_1\mu_2^k \end{bmatrix}, \quad k = 1,2,\dots,d-1.$$

**Proof of Theorem 2.** Let us observe a linear combination $f = \sum_{i=0}^{2d} \gamma_i E_i$. Its restriction to a triangle $T_1$ can be expressed as $f|_{T_1} = \sum_{\boldsymbol{i}\in\mathbb{I}_d} c_{\boldsymbol{i}} B_{\boldsymbol{i}}^{T_1,d}$ where $c_{\boldsymbol{i}} = 0$ for all $\boldsymbol{i} = (i_1,i_2,i_3)$ with $i_3 \ge 2$, while the remaining coefficients depend linearly on the coefficients $\boldsymbol{\gamma} = (\gamma_i)_{i=0}^{2d}$. In more detail, we denote by $A$ the $(2d+1)\times(2d+1)$ matrix, such that

$$A\boldsymbol{\gamma} = \boldsymbol{c}. \tag{14}$$

To prove the linear independency it suffices to show that the matrix $A$ is non-singular. For $d=2$ it equals

$$A = \begin{bmatrix} 1 & 0 & 0 & 0 & 0 \\ \lambda_1 & \lambda_2\xi_2 & \lambda_2\mu_2\xi_1 & \lambda_2\mu_1\xi_1 & 0 \\ 0 & \mu_1\xi_2 & \mu_2\xi_1+\mu_2\xi_2 & \mu_1\xi_1 & 0 \\ 0 & \lambda_1\mu_1\xi_2 & \lambda_1\mu_2\xi_2 & \lambda_1\xi_1 & \lambda_2 \\ 0 & 0 & 0 & 0 & 1 \end{bmatrix}$$

and is nonsingular since $\det A = \lambda_1\lambda_2\mu_2^2\xi_1\xi_2 \ne 0$. Note also that the rows of $A$ sum to one, confirming the partition of unity property.

For $d \ge 3$ one can see from (11) that the matrix $A$ can be split into three parts column-wise (here the Matlab writing conventions for dealing with rows and columns are used):

$$\widetilde{A}_1 = A(:,1:2\ell_1+1), \quad \widetilde{A}_2 = A(:,2\ell_1+2:2(d-\ell_2)), \quad \widetilde{A}_3 = A(:,2(d-\ell_2)+1:2d+1),$$

where

$$\widetilde{A}_1 = \boldsymbol{C}^{Q_2}(:, 1 : 2\ell_1 + 1), \quad \widetilde{A}_3 = \boldsymbol{C}^{Q_1}(:, 2(d - \ell_2) : 2d)$$

and

$$\widetilde{A}_2 = \xi_2 \left[ \boldsymbol{C}^{Q_2}(:, 2\ell_1 + 2 : 2(d - \ell_2 - 1) + 1) \;\middle|\; \begin{matrix} 0 \\ \vdots \\ 0 \end{matrix} \right] + \xi_1 \left[ \begin{matrix} 0 \\ \vdots \\ 0 \end{matrix} \;\middle|\; \boldsymbol{C}^{Q_1}(:, 2\ell_1 + 2 : 2(d - \ell_2 - 1) + 1) \right].$$

Furthermore, the matrix $A$ has the structure

$$A = \left[ \begin{array}{c|c|c} A_1 & & \\ \hline & A_2 & \\ \hline & & A_3 \end{array} \right],$$

where $A_1 \in \mathbb{R}^{(2\ell_1+1)\times(2\ell_1+1)}$ is lower triangular, $A_3 \in \mathbb{R}^{(2\ell_2+1)\times(2\ell_2+1)}$ is upper triangular, and $A_2 \in \mathbb{R}^{5\times5}$ is equal to

$$A_2 = \begin{bmatrix} \lambda_2\xi_2 & 0 & 0 & 0 & 0 \\ \multicolumn{2}{c}{\multirow{2}{*}{$\boxed{\xi_2 M^2_{\ell_1+1}}$}} & 0 & 0 & 0 \\ & & \lambda_2\xi_2 & 0 & 0 \\ 0 & 0 & \multicolumn{2}{c}{\multirow{2}{*}{$\boxed{\xi_2 M^2_{\ell_1+2}}$}} & 0 \\ 0 & 0 & & & 0 \end{bmatrix} + \begin{bmatrix} 0 & \multicolumn{2}{c}{\multirow{2}{*}{$\boxed{\xi_1 M^1_{\ell_2+2}}$}} & 0 & 0 \\ 0 & & & 0 & 0 \\ 0 & 0 & \lambda_1\xi_1 & \multicolumn{2}{c}{\multirow{2}{*}{$\boxed{\xi_1 M^1_{\ell_2+1}}$}} \\ 0 & 0 & 0 & & \\ 0 & 0 & 0 & 0 & \lambda_1\xi_1 \end{bmatrix}$$

$$= \begin{bmatrix} \lambda_2\xi_2 & \lambda_2\mu_2^{\ell_2+2}\xi_1 & \lambda_2(1-\mu_2^{\ell_2+2})\xi_1 & 0 & 0 \\ (1-\mu_2^{\ell_1+1})\xi_2 & \mu_2^{\ell_1+1}\xi_2 + \mu_2^{\ell_2+2}\xi_1 & (1-\mu_2^{\ell_2+2})\xi_1 & 0 & 0 \\ \lambda_1(1-\mu_2^{\ell_1+1})\xi_2 & \lambda_1\mu_2^{\ell_1+1}\xi_2 & \lambda_2\xi_2 + \lambda_1\xi_1 & \lambda_2\mu_2^{\ell_2+1}\xi_1 & \lambda_2(1-\mu_2^{\ell_2+1})\xi_1 \\ 0 & 0 & (1-\mu_2^{\ell_1+2})\xi_2 & \mu_2^{\ell_1+2}\xi_2 + \mu_2^{\ell_2+1}\xi_1 & (1-\mu_2^{\ell_2+1})\xi_1 \\ 0 & 0 & \lambda_1(1-\mu_2^{\ell_1+2})\xi_2 & \lambda_1\mu_2^{\ell_1+2}\xi_2 & \lambda_1\xi_1 \end{bmatrix}.$$

It is straightforward to compute the determinants

$$\det A_1 = \lambda_2^{\ell_1}\mu_2^{\frac{\ell_1(\ell_1+1)}{2}} \quad \det A_3 = \lambda_1^{\ell_2}\mu_2^{\frac{\ell_2(\ell_2+1)}{2}}, \quad \det A_2 = \lambda_1\lambda_2\mu_2^{d+1}\xi_1\xi_2(\lambda_1\xi_1^2\mu_2^{\ell_2} + \lambda_2\xi_2^2\mu_2^{\ell_1} + \xi_1\xi_2\mu_2^{d-1}).$$

Since $\det A = \det A_1 \cdot \det A_2 \cdot \det A_3 > 0$, the matrix $A$ is nonsingular. The given basis functions are non-negative by the construction, and from the structure of the matrix $A$ it is straightforward to see that the rows sum to one, which proves the partition of unity property. □

**Remark 5.** Theorem 2 establishes that any choice of values $\xi_1, \xi_2 \in (0, 1)$ satisfying $\xi_1 + \xi_2 = 1$ yields the B–spline–like edge basis functions. However, the objective is to select these values so that both the condition number of the matrix $A$ (see (14)) and the maximal distance of the Greville points (associated with basis functions $(E_i)_{i=0}^{2d}$) from the edge $\boldsymbol{e} = (\boldsymbol{S}_1, \boldsymbol{S}_2)$ is as small as possible. We denote these two quantities by $\kappa_2$ and `dist`, respectively. Numerical experiments conducted on various triangle configurations indicated that the choice $\xi_1 = \lambda_2$ and $\xi_2 = \lambda_1$ gives near-optimal results.

**Remark 6.** The Greville points associated with the basis functions $(E_i)_{i=0}^{2d}$ can be computed as the solution of the linear system (14) where $\boldsymbol{c}$ is given by (13) with $c_{(i,j,k)} = \boldsymbol{X}^{T_1,d}_{(i,j,k)}$ (see (2)) component-wise.

Next, we demonstrate the proposed construction through numerical examples and provide a comparison with the edge basis functions introduced in [9]. In particular, we compare the condition numbers $\kappa_2$ and the maximal distances `dist`. For all examples we choose $\xi_1 = \lambda_2$ and $\xi_2 = \lambda_1$.

**Example 1.** Let the triangles $T_1$ and $T_2$ be given by $\boldsymbol{S}_1 = (0, 0)$, $\boldsymbol{S}_2 = (1, 0)$, $\boldsymbol{R}_1 = (0.35, 0.5)$, $\boldsymbol{R}_2 = (0, 65, -0.3)$ (see Fig. 3). For this configuration $\sigma_1 = 0.74$, $\sigma_2 = 0.86$, $\rho = -0.6$, $\lambda_1 = 0.4625$, $\lambda_2 = 0.5375$, $\mu_1 = 0.375$, $\mu_2 = 0.625$. For $d = 7$ the basis functions $(E_i)_{i=0}^{2d}$ are shown in Fig. 9.

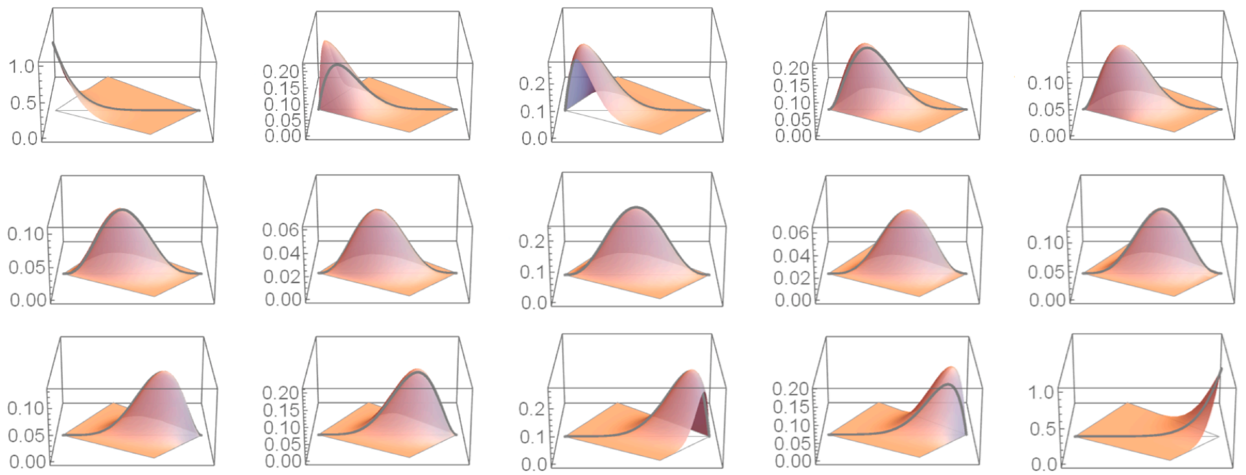

**Fig. 9.** The new $C^1$ basis splines for $d = 7$ over $T_1 \cup T_2$.

**Table 1**
A numerical comparison of condition numbers and maximal Greville point distance from the common edge for our $C^1$ basis and the $C^1$ basis from [9] for fixed triangles $T_1, T_2$ and different degrees $d$.

| | | | | | $T_1 \longleftrightarrow T_2$ $(\mu_2 < \mu_1)$ | | | |
|---|---|---|---|---|---|---|---|---|
| | new basis | | basis from [9] | | new basis | | basis from [9] | |
| d | $\kappa_2$ | dist | $\kappa_2$ | dist | $\kappa_2$ | dist | $\kappa_2$ | dist |
| 2 | 8.3140 | 1.0057 | 11.962 | 2.0448 | 13.860 | 1.0057 | 17.795 | 1.8437 |
| 3 | 7.7977 | 0.6165 | 38.978 | 4.1318 | 21.162 | 0.98771 | 79.491 | 5.6168 |
| 4 | 11.284 | 0.6573 | 27.419 | 2.7223 | 36.143 | 1.7140 | 34.272 | 2.1277 |
| 5 | 12.370 | 0.6254 | 35.262 | 2.0206 | 59.752 | 1.8725 | 64.992 | 2.9096 |
| 6 | 18.375 | 0.8780 | 52.862 | 3.6758 | 100.79 | 3.3877 | 55.601 | 2.4692 |
| 7 | 19.866 | 0.8495 | 36.485 | 1.3400 | 165.82 | 3.7744 | 60.749 | 2.0319 |
| 8 | 30.095 | 1.1894 | 94.260 | 5.0206 | 288.69 | 7.0352 | 83.379 | 2.8802 |
| 9 | 32.574 | 1.1625 | 38.932 | 1.0273 | 470.42 | 7.9898 | 59.074 | 1.5863 |

Fig. 10 illustrates the comparison between the Greville points associated with the basis functions $(E_i)_{i=0}^{2d}$ (green) with those derived in [9] (orange) for degrees $d = 2, 3, \ldots, 8$. A detailed numerical comparison of these two bases – considering the condition numbers $\kappa_2$ of the corresponding matrices and the maximal distances `dist` of the Greville points from the edge is provided in Table 1 (columns 2–5), which indicates that the new basis performs much better.

Note that for the chosen triangles $T_1$ and $T_2$, the barycentric coordinates $\mu_1$ and $\mu_2$ are such that $\mu_2 > \mu_1$. If we exchange the ordering of the triangles (see Remark 3), i.e., we exchange $\boldsymbol{R}_1$ and $\boldsymbol{R}_2$, which yields $\mu_1 > \mu_2$, the obtained basis functions $(E_i)_{i=0}^{2d}$ (as well as basis functions from [9]) have much worse properties in terms of $\kappa_2$ and `dist` as indicated in Table (columns 6–9). Furthermore, numerical experiments conducted on several other triangle configurations indicated that the order of the two triangles in the construction of the basis should be such that $\mu_2 \geq \mu_1$. In addition, Table 2 presents the values of $\kappa_2$ and `dist` obtained when the first two vertices of $Q_1$ are exchanged (first two columns) and when the first two vertices of $Q_2$ are exchanged (last two columns). The results show that these alternative choices lead to worse numerical properties, which is in agreement with the observation in Remark 4.

As can be seen from Table 1, the purely algebraic construction from [9] appears to be more robust with respect to the ordering of the two triangles than the construction proposed here, in which different orderings of the triangles result in different couplings of Bernstein basis polynomials (see Remark 3). Nevertheless, when the ordering is chosen such that $\mu_2 \geq \mu_1$, the new construction outperforms that of [9] with respect to the considered criteria, as illustrated by the next example.

**Example 2.** We now compare the basis $(E_i)_{i=0}^{2d}$, defined in (11), with the basis proposed in [9] for fixed polynomial degrees $d = 6$ and $d = 7$, considering different triangle configurations (such that $\mu_2 \geq \mu_1$). The vertices of the triangles are chosen as $\boldsymbol{S}_1 = (0, 0)$, $\boldsymbol{S}_2 = (1, 0)$, $\boldsymbol{R}_1 = (0.5, 1)$, $\boldsymbol{R}_2 = (\frac{1}{6}(8\alpha - 1), -\frac{1}{3})$ for $\alpha \in \{0.1, 0.2, 0.3, 0.4, 0.5\}$ (see Fig. 11, left). Note that $\lambda_1 = 1 - \alpha$, while $\mu_1 = 0.25$ is fixed. Table 3 (first five rows) reports the values $\kappa_2$ and `dist` for both the basis (11) and the basis from [9]. The results indicate that the new basis outperforms the previously introduced one across the tested configurations. Similarly, Table 3 (last five rows) shows the results for $\boldsymbol{R}_2 = \frac{1}{\alpha - 1}(\frac{\alpha}{2} - \frac{1}{3}, \alpha)$ (see Fig. 11, right), for which $\lambda_1 = \frac{2}{3}$ is fixed and $\mu_1 = \alpha$.

From Table 3 one can observe that the condition number and the distance of the Greville points from the edge increase as the configuration approaches the limiting case $\lambda_1 \to 1$ (equivalently, $\lambda_2 \to 0$). This behavior can be intuitively explained by the geometry

**Table 2**
Condition numbers and maximal Greville point distance from the common edge for the $C^1$ basis when the first two vertices of $Q_1$ are exchanged (first two columns) and when the first two vertices of $Q_2$ are exchanged (last two columns), for the triangles $T_1, T_2$ from Example 1 and different degrees $d$.

| | $Q_{1,1} \longleftrightarrow Q_{1,2}$ | | $Q_{2,1} \longleftrightarrow Q_{2,2}$ | |
|---|---|---|---|---|
| $d$ | $\kappa_2$ | dist | $\kappa_2$ | dist |
| 2 | 9.9307 | 1.8705 | 9.8164 | 1.7498 |
| 3 | 97.840 | 8.7446 | 50.903 | 4.8703 |
| 4 | 189.80 | 12.661 | 35.086 | 2.4113 |
| 5 | 76.394 | 4.5641 | 53.337 | 2.8869 |
| 6 | 199.81 | 9.4486 | 77.042 | 3.0263 |
| 7 | 123.83 | 5.3766 | 92.019 | 3.5803 |
| 8 | 193.19 | 7.6846 | 197.44 | 5.2749 |
| 9 | 277.92 | 8.0894 | 213.01 | 5.5029 |

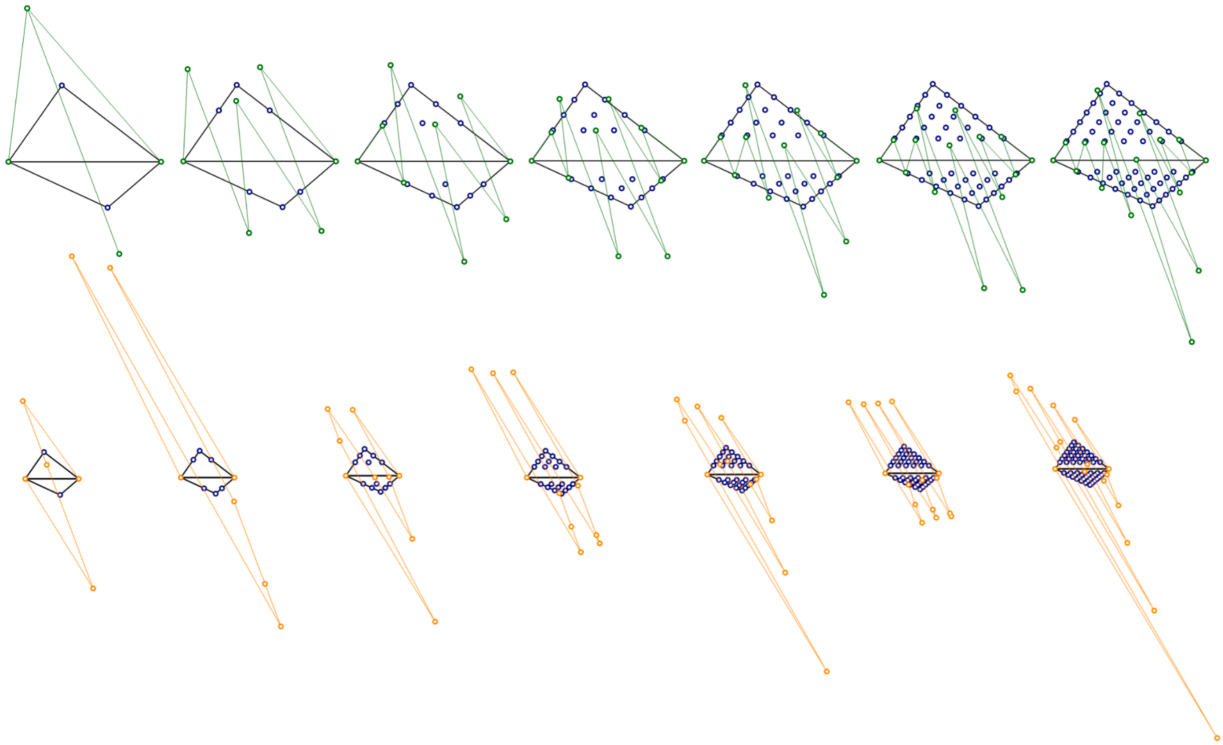

**Fig. 10.** A comparison of Greville points obtained for the new basis (green) and for the basis from [9] (orange) for degrees $d = 2, 3, \ldots, 8$.

of the control triangles, since, as follows from (7), the area of the control triangle $Q_2$ grows proportionally to $\frac{1}{\lambda_2}$. A similar behavior occurs for $\lambda_1 \to 0$. A more detailed theoretical analysis is beyond the scope of the present paper. Nevertheless, this observation indicates that, when applying the basis construction to a full triangulation, one should avoid pairs of triangles that are close to such limiting configurations, for instance by introducing additional splittings. In particular, the intersection point $\boldsymbol{Z}$ (see (6)) should remain sufficiently close to the midpoint of the common edge.

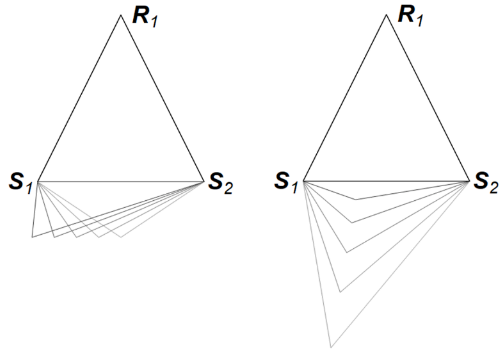


**Fig. 11.** Various triangle configurations used for the comparison shown in Table 3. The triangles on the left correspond to the first 5 rows and the ones on the right corresponds to the last 5 rows of numerical values.

**Table 3**
A numerical comparison of condition numbers $\kappa_2$ and maximal distances of Greville points from the common edge for our $C^1$ basis and the $C^1$ basis from [9] with degrees $d = 6$ and $d = 7$ for different triangle configurations, shown in Fig. 11. The first five rows correspond to positions with a fixed $\mu_1 = 0.25$ and different values of $\lambda_1$. The last five rows show results as $\mu_1$ changes and $\lambda_1 = 2/3$ is fixed.

| | | | $d = 6$ | | | | $d = 7$ | | | |
|---|---|---|---|---|---|---|---|---|---|---|
| | | | new basis | | basis from [9] | | new basis | | basis from [9] | |
| $\boldsymbol{R}_2$ | $\lambda_1$ | $\mu_1$ | $\kappa_2$ | dist | $\kappa_2$ | dist | $\kappa_2$ | dist | $\kappa_2$ | dist |
| $(-1/30, -1/3)$ | 0.9 | 0.25 | 50.880 | 2.4584 | 236.07 | 25.978 | 55.416 | 2.1739 | 272.50 | 23.766 |
| $(1/10, -1/3)$ | 0.8 | 0.25 | 22.417 | 1.3340 | 41.331 | 5.4564 | 24.210 | 1.1879 | 109.62 | 9.8889 |
| $(7/30, -1/3)$ | 0.7 | 0.25 | 14.290 | 0.97604 | 33.225 | 4.5391 | 15.125 | 0.88531 | 94.064 | 8.7529 |
| $(11/30, -1/3)$ | 0.6 | 0.25 | 11.204 | 0.82983 | 57.918 | 8.1071 | 11.614 | 0.75379 | 85.052 | 9.2718 |
| $(1/2, -1/3)$ | 0.5 | 0.25 | 10.173 | 0.83515 | 113.34 | 15.587 | 10.460 | 0.70018 | 129.99 | 14.260 |
| $(17/54, -1/9)$ | 2/3 | 0.1 | 7.7146 | 0.79136 | 472.56 | 60.342 | 7.9601 | 0.69311 | 1777.9 | 195.42 |
| $(7/24, -1/4)$ | 2/3 | 0.2 | 10.396 | 0.84081 | 65.468 | 9.0066 | 11.032 | 0.75637 | 139.31 | 15.962 |
| $(11/42, -3/7)$ | 2/3 | 0.3 | 16.845 | 1.2877 | 28.947 | 3.9138 | 17.418 | 1.1746 | 74.987 | 7.9998 |
| $(2/9, -2/3)$ | 2/3 | 0.4 | 31.916 | 2.5052 | 35.580 | 4.8963 | 32.916 | 2.2901 | 41.314 | 4.8451 |
| (1/6,-1) | 2/3 | 0.5 | 66.875 | 4.9500 | 71.919 | 9.4479 | 71.480 | 4.7773 | 29.921 | 3.0837 |

**Remark 7.** The edge basis functions derived in this section can be employed in exactly the same manner as the splines introduced in [9] for constructing the B–spline–like basis of the Argyris spline space [9, Section 3] and generalized Clough–Tocher spline space of arbitrary degree [23].

## 5. $C^2$ Continuous B–spline–like basis functions

For $r = 2$ the definition (9) provides $3(d-1)$ spline functions

$$\boldsymbol{\varphi}^{Q_j} := \left\{ \varphi_{0,1}^{Q_j}, \varphi_{1,1}^{Q_j}, \varphi_{1,2}^{Q_j} \right\} \cup \left\{ \varphi_{k,1}^{Q_j}, \varphi_{k,2}^{Q_j}, \varphi_{k,3}^{Q_j} \;:\; k = 2, 3, \ldots, d-2 \right\} \cup \left\{ \varphi_{d-1,1}^{Q_j}, \varphi_{d-1,2}^{Q_j}, \varphi_{d,1}^{Q_j} \right\} \tag{15}$$

for each control triangle $Q_j$, $j = 1, 2$, where the first three and the last three splines belong to a group of vertex basis functions, while the remaining $3(d-3)$ are the candidates for $3(d-2)$ edge basis splines, which we need to determine. To observe the restriction of these splines to the triangle $T_1$ or $T_2$, we collect the nonzero Bézier coefficients (i.e., coefficients $c_{(i_1,i_2,i_3)}$ with $i_3 \leq 2$) into a vector of the form

$$\boldsymbol{c} = \left( c_{(d,0,0)}, c_{(d-1,0,1)}, c_{(d-1,1,0)}, \left( c_{(d-k,k-2,2)}, c_{(d-k,k-1,1)}, c_{(d-k,k,0)} \right)_{k=2}^{d} \right)^T. \tag{16}$$

Since the Bézier coefficients with $i_3 \leq 2$ over $T_1$ are uniquely determined by those over $T_2$ via the $C^2$ continuity conditions, and vise-versa, we restrict the analysis to the triangle $T_1$. The next lemma follows directly using the results given in Theorem 1.

**Lemma 3.** *Let $\boldsymbol{C}^{Q_j}$ denote the $3d \times 3(d-1)$ matrix with columns that correspond to values of Bézier coefficients (16) of splines in the ordered set $\boldsymbol{\varphi}^{Q_j}$ (given by (15)) restricted to $T_1$. The two matrices are equal to*

$$
\boldsymbol{C}^{Q_1} = \left[\begin{array}{c|c|c|c|c}
\boldsymbol{M}^1_{d-1} & & & & \\ \hline
\boldsymbol{N}^1_{d-1} & \boldsymbol{M}^1_{d-2} & & & \\ \hline
\lambda_1^2 & \boldsymbol{N}^1_{d-2} & \ddots & & \\ \hline
 & \lambda_1^2 & \ddots & \boldsymbol{M}^1_2 & \\ \hline
 & & \lambda_1^2 & \boldsymbol{N}^1_2 & \boldsymbol{M}^1_1 \\ \hline
 & & & \lambda_1^2 & \boldsymbol{N}^1_1
\end{array}\right], \quad
\boldsymbol{C}^{Q_2} = \left[\begin{array}{c|c|c|c|c}
1 & & & & \\ \hline
\boldsymbol{M}^2_1 & \lambda_2^2 & & & \\ \hline
\boldsymbol{N}^2_1 & \boldsymbol{M}^2_2 & \lambda_2^2 & & \\ \hline
 & \boldsymbol{N}^2_2 & \ddots & \lambda_2^2 & \\ \hline
 & & \ddots & \boldsymbol{M}^2_{d-2} & \lambda_2^2 \\ \hline
 & & & \boldsymbol{N}^2_{d-2} & \boldsymbol{M}^2_{d-1} \\ \hline
 & & & & \boldsymbol{N}^2_{d-1}
\end{array}\right],
$$

*where*

$$
\boldsymbol{M}^1_\ell = \begin{bmatrix} \lambda_2^2 \\ \lambda_2 \\ 1 \end{bmatrix} \cdot \left[\mu_2^\ell, \ell\mu_1\mu_2^{\ell-1}, 1-\mu_2^\ell - \ell\mu_1\mu_2^{\ell-1}\right], \quad \ell = 1,2,\ldots,d-2,
$$

$$
\boldsymbol{M}^1_{d-1} = \begin{bmatrix} 1 & 0 & 0 \\ \lambda_1 & \lambda_2\mu_2^{d-1} & \lambda_2(1-\mu_2^{d-1}) \\ 0 & \mu_2^{d-1} & 1-\mu_2^{d-1} \end{bmatrix}, \quad
\boldsymbol{N}^1_1 = \begin{bmatrix} 0 & 2\lambda_1\lambda_2 & \lambda_2^2 \\ 0 & \lambda_1 & \lambda_2 \\ 0 & 0 & 1 \end{bmatrix}, \quad
\boldsymbol{N}^1_{d-1} = \begin{bmatrix} \lambda_1^2 & 0 & 2\lambda_1\lambda_2 \\ 0 & 0 & \lambda_1 \\ 0 & 0 & 0 \end{bmatrix},
$$

$$
\boldsymbol{N}^1_\ell = \begin{bmatrix} 2\lambda_1\lambda_2 \\ \lambda_1 \\ 0 \end{bmatrix} \cdot \left[0, \mu_2^{\ell-1}, 1-\mu_2^{\ell-1}\right], \quad \ell = 2,3,\ldots,d-2,
$$

*and*

$$
\boldsymbol{M}^2_1 = \begin{bmatrix} \lambda_1 & \lambda_2 & 0 \\ 0 & \mu_1 & \mu_2 \\ \lambda_1^2 & 2\lambda_1\lambda_2 & 0 \end{bmatrix}, \quad
\boldsymbol{M}^2_\ell = \begin{bmatrix} \lambda_2(1-\mu_2^{\ell-1}) & \lambda_2\mu_2^{\ell-1} & 0 \\ 1-\ell\mu_1\mu_2^{\ell-1}-\mu_2^\ell & \ell\mu_1\mu_2^{\ell-1} & \mu_2^\ell \\ 2\lambda_1\lambda_2(1-\mu_2^{\ell-1}) & 2\lambda_1\lambda_2\mu_2^{\ell-1} & 0 \end{bmatrix}, \quad \ell = 2,3,\ldots,d-2,
$$

$$
\boldsymbol{M}^2_{d-1} = \begin{bmatrix} \lambda_2 & 0 & 0 \\ 1-\mu_2^{d-1} & \mu_2^{d-1} & 0 \\ 2\lambda_1\lambda_2 & 0 & \lambda_2^2 \end{bmatrix}, \quad
\boldsymbol{N}^2_\ell = \begin{bmatrix} \lambda_1 \\ 0 \\ \lambda_1^2 \end{bmatrix} \cdot \left[1-\ell\mu_1\mu_2^{\ell-1}-\mu_2^\ell, \ell\mu_1\mu_2^{\ell-1}, \mu_2^\ell\right], \quad \ell = 1,2,\ldots,d-2,
$$

$$
\boldsymbol{N}^2_{d-1} = \begin{bmatrix} \lambda_1(1-\mu_2^{d-1}) & \lambda_1\mu_2^{d-1} & \lambda_2 \\ 0 & 0 & 1 \end{bmatrix}.
$$

*Their rows sum to one.*

For a group of vertex basis splines we select

$$
E_0 := \varphi^{Q_2}_{0,1}, \quad E_1 := \varphi^{Q_2}_{1,1}, \quad E_2 := \varphi^{Q_2}_{1,2}, \quad E_{3d-3} := \varphi^{Q_1}_{d-1,1}, \quad E_{3d-2} := \varphi^{Q_1}_{d-1,2}, \quad E_{3d-1} := \varphi^{Q_1}_{d,1}. \tag{17a}
$$

Since we need $3(d-2)$ linearly independent edge basis splines, but we get only $3(d-3)$ such splines from each of the control triangles $Q_1$ and $Q_2$, we must again combine these splines with the aim to keep as many as possible "uncombined" splines. For $d \geq 5$ the choice that we propose is the following:

$$
\begin{aligned}
&E_{3i-3} = \varphi^{Q_2}_{i,1}, \quad E_{3i-2} = \varphi^{Q_2}_{i,2}, \quad E_{3i-1} = \varphi^{Q_2}_{i,3}, \quad i = 2,\ldots,\ell_1+1, \\
&E_{3\ell_1+3} = \xi_2\varphi^{Q_2}_{\ell_1+2,1}, \quad E_{3\ell_1+4} = \xi_1\varphi^{Q_1}_{\ell_1+2,1}, \quad E_{3\ell_1+5} = \xi_2\varphi^{Q_2}_{\ell_1+2,2}, \\
&E_{3\ell_1+6} = \xi_1\varphi^{Q_1}_{\ell_1+2,2} + \xi_2\varphi^{Q_2}_{\ell_1+2,3}, \quad E_{3\ell_1+7} = \xi_1\varphi^{Q_1}_{\ell_1+2,3} + \xi_2\varphi^{Q_2}_{\ell_1+3,1}, \quad E_{3\ell_1+8} = \xi_1\varphi^{Q_1}_{\ell_1+3,1} + \xi_2\varphi^{Q_2}_{\ell_1+3,2}, \\
&E_{3\ell_1+9} = \xi_1\varphi^{Q_1}_{\ell_1+3,2}, \quad E_{3\ell_1+10} = \xi_2\varphi^{Q_2}_{\ell_1+3,3}, \quad E_{3\ell_1+11} = \xi_1\varphi^{Q_1}_{\ell_1+3,3}, \\
&E_{3i} = \varphi^{Q_1}_{i,1}, \quad E_{3i+1} = \varphi^{Q_1}_{i,2}, \quad E_{3i+2} = \varphi^{Q_1}_{i,3}, \quad i = d-1-\ell_2,\ldots,d-2,
\end{aligned} \tag{17b}
$$

where

$$
\text{(a) } \ell_1 = \left\lceil \tfrac{d-5}{2} \right\rceil, \; \ell_2 = d-5-\ell_1, \quad \text{(b) } \ell_1 = \left\lfloor \tfrac{d-5}{2} \right\rfloor, \; \ell_2 = d-5-\ell_1, \tag{18}
$$

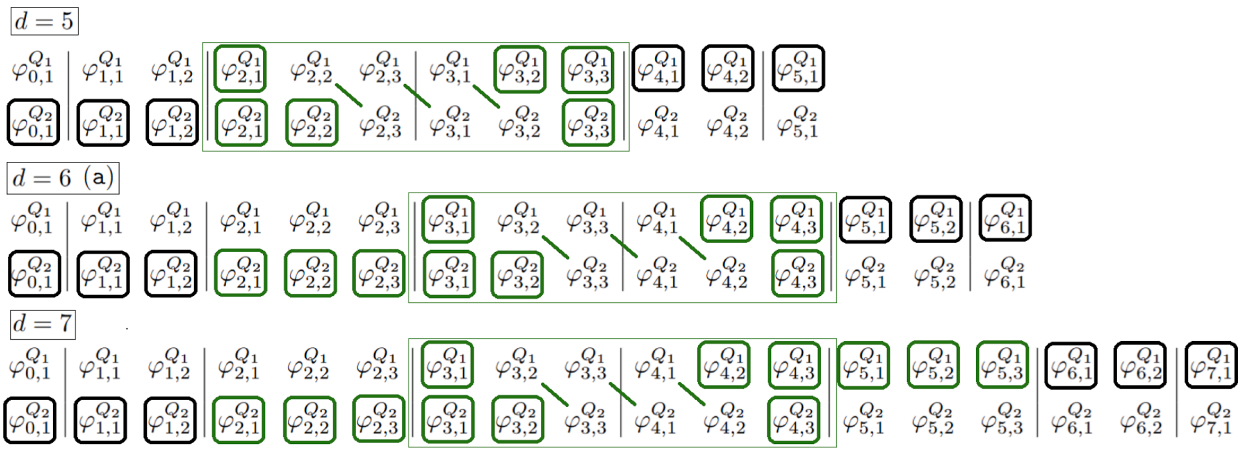


**Fig. 12.** An illustration of the 2nd coupling for $C^2$, done similarly to the $C^1$ case.

and $\xi_1, \xi_2 \in (0,1)$, $\xi_1 + \xi_2 = 1$, are any two chosen parameters. Note that for odd degrees $d$ both choices are the same. A graphical illustration of this proposed coupling for $d = 5$, $d = 6\,(\mathrm{a})$ and $d = 7$ is shown in Fig. 12. Black border quadrilaterals indicate the selected vertex basis functions. Green border quadrilaterals represent splines that are individually included in the edge group, while green connecting lines signify that a convex combination of two splines is included in the edge group. Thin green border quadrilaterals denote that each function in the first row is multiplied by $\xi_1$ and each function in the second row by $\xi_2$.

The degree $d = 4$ requires a special analysis due to fact that the union of the 6 edge splines obtained from both control triangles is not linearly independent. Namely, one can check that

$$\varphi_{2,1}^{Q_1} + \varphi_{2,2}^{Q_1} + \varphi_{2,3}^{Q_1} = \varphi_{2,1}^{Q_2} + \varphi_{2,2}^{Q_2} + \varphi_{2,3}^{Q_2},$$

thus we need to find one additional $C^2$ spline to be added to the edge group. It is straightforward to see that

$$\varphi_{2,0}(\boldsymbol{X}) = \begin{cases} 2\lambda_1\lambda_2\mu_2^2\, B_{(1,1,2)}^{T_1,4}(\boldsymbol{X}), & \boldsymbol{X} \in T_1 \\ 2\lambda_1\lambda_2\mu_1^2\, B_{(1,1,2)}^{T_2,4}(\boldsymbol{X}), & \boldsymbol{X} \in T_2 \end{cases}$$

is $C^2$ continuous, non-negative, and it clearly belongs to the edge group. Defining

$$E_3 = \xi_2\varphi_{2,1}^{Q_2}, \quad E_4 = \xi_1\varphi_{2,1}^{Q_1}, \quad E_5 = \xi_1\varphi_{2,2}^{Q_1} + \xi_2\varphi_{2,2}^{Q_2} - \varphi_{2,0}, \quad E_6 = \varphi_{2,0}, \quad E_7 = \xi_2\varphi_{2,3}^{Q_2}, \quad E_8 = \xi_1\varphi_{2,3}^{Q_1} \tag{19}$$

provides 6 non-negative linearly independent edge B–spline–like basis functions as proven in the following lemma.

**Theorem 3.** *Let $d = 4$ and let $\xi_1, \xi_2 \in (0,1)$, $\xi_1 + \xi_2 = 1$, be any two chosen parameters. The splines $E_i$, $i = 0,1,2,9,10,11$, defined by (17a), and $E_i$, $i = 3,4,5,6,7,8$, defined by (19), are linearly independent, satisfy the partition of unity property, and are non-negative over $T_1 \cup T_2$.*

**Proof.** Let $A \in \mathbb{R}^{12\times 12}$ be the matrix with columns that correspond to values of Bézier coefficients (16) of splines $(E_i)_{i=0}^{11}$ restricted to $T_1$. It equals

$$\begin{bmatrix}
1 & 0 & 0 & 0 & 0 & 0 & 0 & 0 & 0 & 0 & 0 & 0 \\
\lambda_1 & \lambda_2 & 0 & 0 & 0 & 0 & 0 & 0 & 0 & 0 & 0 & 0 \\
0 & \mu_1 & \mu_2 & 0 & 0 & 0 & 0 & 0 & 0 & 0 & 0 & 0 \\
\lambda_1^2 & 2\lambda_1\lambda_2 & 0 & \lambda_2^2\xi_2 & \lambda_2^2\mu_2^2\xi_1 & 2\lambda_2^2\mu_1\mu_2\xi_1 & 0 & 0 & \lambda_2^2\mu_1^2\xi_1 & 0 & 0 & 0 \\
0 & \lambda_1\mu_1 & \lambda_1\mu_2 & \lambda_2\mu_1\xi_2 & \lambda_2\mu_2^2\xi_1 & \lambda_2\mu_2\left(2\mu_1\xi_1 + \xi_2\right) & 0 & 0 & \lambda_2\mu_1^2\xi_1 & 0 & 0 & 0 \\
0 & 0 & 0 & \mu_1^2\xi_2 & \mu_2^2\xi_1 & 2\mu_1\mu_2 & 0 & \mu_2^2\xi_2 & \mu_1^2\xi_1 & 0 & 0 & 0 \\
0 & \lambda_1^2\mu_1 & \lambda_1^2\mu_2 & 2\lambda_1\lambda_2\mu_1\xi_2 & 0 & 2\lambda_1\lambda_2\mu_1\mu_2 & 2\lambda_1\lambda_2\mu_2^2 & 0 & 2\lambda_1\lambda_2\mu_1\xi_1 & \lambda_2^2\mu_2 & \lambda_2^2\mu_1 & 0 \\
0 & 0 & 0 & \lambda_1\mu_1^2\xi_2 & 0 & \lambda_1\mu_2\left(2\mu_1\xi_2 + \xi_1\right) & 0 & \lambda_1\mu_2^2\xi_2 & \lambda_1\mu_1\xi_1 & \lambda_2\mu_2 & \lambda_2\mu_1 & 0 \\
0 & 0 & 0 & 0 & 0 & 0 & 0 & 0 & 0 & \mu_2 & \mu_1 & 0 \\
0 & 0 & 0 & \lambda_1^2\mu_1^2\xi_2 & 0 & 2\lambda_1^2\mu_1\mu_2\xi_2 & 0 & \lambda_1^2\mu_2^2\xi_2 & \lambda_1^2\xi_1 & 0 & 2\lambda_1\lambda_2 & \lambda_2^2 \\
0 & 0 & 0 & 0 & 0 & 0 & 0 & 0 & 0 & 0 & \lambda_1 & \lambda_2 \\
0 & 0 & 0 & 0 & 0 & 0 & 0 & 0 & 0 & 0 & 0 & 1
\end{bmatrix}$$

and has a nonzero determinant $\det A = 2\lambda_1^5\lambda_2^5\mu_2^{10}\xi_1^2\xi_2^2$. The rows sum to one and the elements are clearly non-negative. It remains to prove that $(E_i)_{i=0}^{11}$ are non-negative over $T_2$ as well (in particular, we must check $E_5$, as the others are non-negative by construction). This follows from the observation that the matrix with Bézier coefficients over $T_2$ equals the matrix $A$ with permuted columns (by applying the permutation $\{1,3,2,8,9,6,7,4,5,11,10,12\}$) and exchanged values of $\mu_1$ and $\mu_2$. This completes the proof. $\square$

**Theorem 4.** *Let $d \geq 5$ and let $\xi_1, \xi_2 \in (0,1)$, $\xi_1 + \xi_2 = 1$, be any two chosen parameters. The splines $E_i$, $i = 0,1,\ldots,3d-1$, defined by (17a) and (17b), are linearly independent, satisfy the partition of unity property, and are non-negative over $T_1 \cup T_2$.*

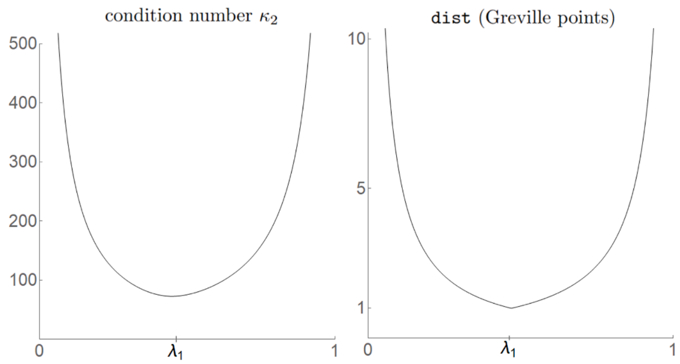


**Fig. 13.** Graphs of $\kappa_2$ (left) and dist (right) as functions of $\xi_2$ for a fixed degree $d = 5$ and the triangles $T_1$ and $T_2$ from Example 3.

**Proof.** The non-negativity over $T_1 \cup T_2$ holds true from the construction. Namely, the Bézier coefficients of splines (15) are clearly non-negative and $E_i$ are just convex combinations of these splines. To prove the linear independency and the partition of unity, we denote – as in the proof of Theorem 3 – by $A$ the matrix with columns that correspond to values of Bézier coefficients (16) of splines $(E_i)_{i=0}^{3d-1}$ restricted to $T_1$. We need to prove that $A$ is nonsingular, and that its rows sum to one. By (17) and Lemma 3 one can see that the columns of $A$ are equal to

$$A(:, 1 : 3(\ell_1 + 1)) = C^{Q_2}(:, 1 : 3(\ell_1 + 1)),$$
$$A(:, 3\ell_1 + 4 : 3\ell_1 + 12) = \xi_1 \widetilde{C}^{Q_1} + \xi_2 \widetilde{C}^{Q_2},$$
$$A(:, 3d - 3(\ell_2 + 1) + 1 : 3d) = C^{Q_1}(:, 3d - 3(\ell_2 + 1) + 1 : 3d),$$

where $\widetilde{C}^{Q_1}$ is the $3d \times 9$ matrix obtained by inserting zero vectors at columns $1, 3, 8$ and sequentially filling the remaining columns with columns from $C^{Q_1}(:, 3\ell_1 + 4 : 3\ell_1 + 9)$, and $\widetilde{C}^{Q_2}$ is the analogous matrix with zero columns $2, 7, 9$ and the rest taken sequentially from $C^{Q_2}(:, 3\ell_1 + 4 : 3\ell_1 + 9)$.

From the structure of the matrix one can observe that the submatrices $A(1 : 3(\ell_1 + 1), 3\ell_1 + 4 : 3d)$ and $A(3d - 3(\ell_2 + 1) + 2 : 3d, 1 : 3d - 3(\ell_2 + 1))$ have zero elements, thus the determinant of $A$ is decomposed into determinants of three diagonal block matrices $\det A = \det A_1 \cdot \det A_2 \cdot \det A_3$, where it is straightforward to compute that

$$\det A_1 = \det C^{Q_2}(1 : 3(\ell_1 + 1), 1 : 3(\ell_1 + 1)) = \lambda_2^{3\ell_1+1} \mu_2^{(\ell_1+1)^2},$$
$$\det A_3 = \det C^{Q_1}(3d - 3(\ell_2 + 1) + 2 : 3d - 3(\ell_2 + 1) + 2 : 3d) = (-1)^{\ell_2} \lambda_1^{3\ell_2+1} \mu_2^{\ell_2(\ell_2+1)},$$

because $A_1$ is lower triangular and $\det A_3$ can be transformed to a lower triangular by shifting its rows. The $10 \times 10$ matrix $A_2$ is a submatrix of $\xi_1 \widetilde{C}^{Q_1} + \xi_2 \widetilde{C}^{Q_2}$ extended by one row and one column to the right. With some elementary computations one can check that its determinant equals

$$\det A_2 = -\lambda_1^5 \lambda_2^5 \xi_1^3 \xi_2^3 \mu_2^{3\ell_1+4\ell_2+15} \left( \lambda_2 \xi_2 \mu_2^{\ell_1} \left( 2\xi_1 \mu_2^{\ell_2+2} + \xi_2 \right) + \lambda_1 \xi_1 \mu_2^{\ell_2} \left( 2\xi_2 \mu_2^{\ell_1+2} + \xi_1 \right) \right).$$

Thus, the determinant of $A$ is clearly nonzero, which confirms the linear independency. It is also straightforward to see that the rows of the matrix $A$ sum to one. This completes the proof. $\square$

**Remark 8.** Let $A$ be the matrix with columns that correspond to values of Bézier coefficients (16) of basis splines $(E_i)_{i=0}^{3d-1}$ restricted to $T_1$ (see the proof of Theorems 3 and 4). The Greville points associated with these basis splines can be computed as the solution of the linear system with a matrix $A$ and the right hand side vector $\boldsymbol{c}$ given by (13) with $c_{(i,j,k)} = \boldsymbol{X}_{(i,j,k)}^{T_1,d}$ (see (2)) component-wise.

**Remark 9.** By Theorems 3 and 4 any choice of values $\xi_1, \xi_2 \in (0,1)$ satisfying $\xi_1 + \xi_2 = 1$, yields B–spline-like edge basis functions. As for $C^1$ continuous basis splines, numerical experiments showed that choosing $\xi_1 = \lambda_2$ and $\xi_2 = \lambda_1$ provides the basis with nearly optimal values of $\kappa_2$ and dist. Furthermore, the numbering/order of triangles $T_1$ and $T_2$ in the construction process should be taken so that $\mu_2 \geq \mu_1$.

As no constructions of $C^2$ edge B–spline–like basis functions of general degree are available in the literature for comparison, we restrict the numerical experiments to demonstrating the properties of the derived basis through representative examples.

**Example 3.** Let the triangles $T_1$ and $T_2$ be chosen as in Example 1. Fig. 13 shows graphs of $\kappa_2$ and dist as functions of $\xi_2$ for a fixed degree $d = 5$. These results numerically confirm that the choice $\xi_2 = \lambda_1$ yields optimal performance – note that the minimum is not attained exactly at $\lambda_1$, but it is close to this value. The basis splines $(E_i)_{i=0}^{3d-1}$ of degree $d = 5$ corresponding to $\xi_2 = \lambda_1$ are depicted in Fig. 14. The values $(\kappa_2, \mathtt{dist})$ for degrees $d = 4, 5, \ldots, 9$ are equal to $(33.866, 1.0057)$, $(72.677, 1.0053)$, $(121.01, 0.89562)$, $(158.98, 0.65958)$, $(248.25, 0.51549)$, $(327.62, 0.59333)$, respectively, and the corresponding Greville points are shown in Fig. 15.

**Example 4.** Let the vertices of the triangles be chosen as in Example 2, i.e., the triangle $T_1$ is fixed while the triangle $T_2$ changes the position as shown in Fig. 11. Table 4 reports the values $\kappa_2$ and dist for the basis (17) of degree $d = 6$ (case (a)) and $d = 7$. The

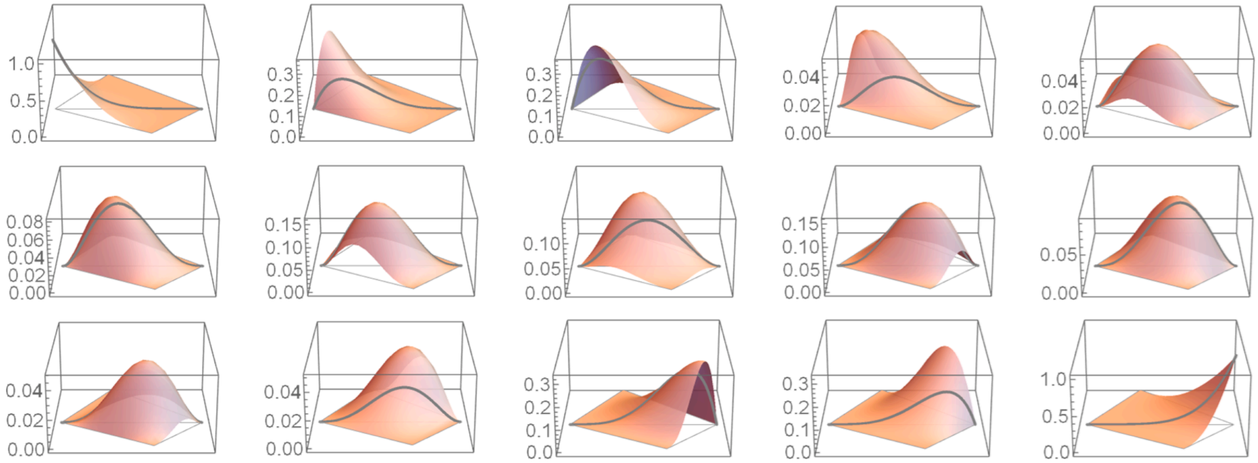
**Fig. 14.** The $C^2$ basis splines $(E_i)_{i=0}^{3d-1}$ for $d = 5$ over $T_1 \cup T_2$ from Example 3.

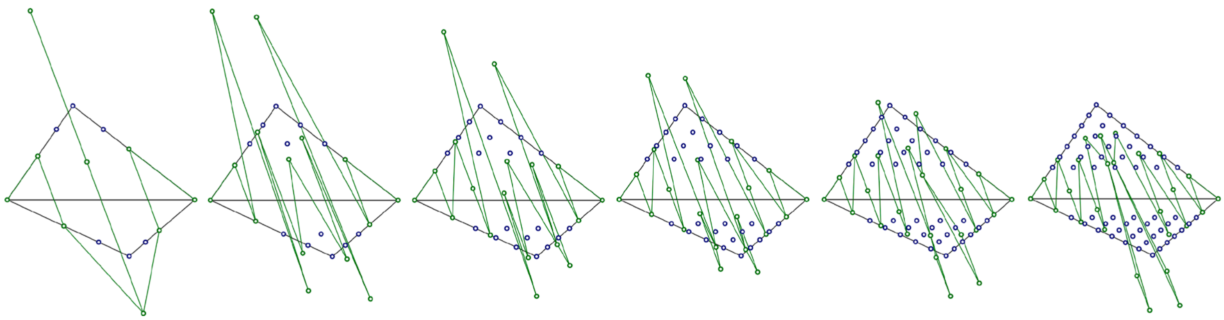
**Fig. 15.** The Greville points associated with the $C^2$ basis splines $(E_i)_{i=0}^{3d-1}$ of degree $d = 4, 5, \ldots, 9$ (left to right).

**Table 4**
Condition numbers and maximal distances of Greville point from the common edge for our $C^2$ basis (17) of degree $d = 6$ and $d = 7$ for different triangle configurations (shown in Fig. 11).

| | | $d=6$ | | $d=7$ | |
|---|---|---|---|---|---|
| $\lambda_1$ | $\mu_1$ | $\kappa_2$ | dist | $\kappa_2$ | dist |
| 0.9 | 0.25 | 989.91 | 4.6539 | 992.24 | 4.3610 |
| 0.8 | 0.25 | 233.08 | 2.5450 | 235.09 | 2.3695 |
| 0.7 | 0.25 | 104.38 | 1.8864 | 107.03 | 1.7435 |
| 0.6 | 0.25 | 63.934 | 1.6942 | 68.363 | 1.4730 |
| 0.5 | 0.25 | 48.808 | 1.6967 | 57.224 | 1.3651 |
| | | $d=6$ | | $d=7$ | |
| $\lambda_1$ | $\mu_1$ | $\kappa_2$ | dist | $\kappa_2$ | dist |
| 2/3 | 0.1 | 34.829 | 1.7397 | 34.940 | 1.5454 |
| 2/3 | 0.2 | 61.605 | 1.7588 | 63.149 | 1.6092 |
| 2/3 | 0.3 | 123.90 | 1.7951 | 129.56 | 1.6268 |
| 2/3 | 0.4 | 276.99 | 1.7973 | 293.82 | 1.4744 |
| 2/3 | 0.5 | 702.15 | 1.6818 | 747.04 | 1.8000 |

results indicate that the basis performs well across a broad range of triangle configurations, including cases in which the geometry approaches limiting configurations where the two triangles would no longer form a convex quadrilateral. Nevertheless, since the areas of the control triangles grow as $\lambda_1 \to 0$ or $\lambda_2 \to 0$ (see (7)), one may still expect $\kappa_2$ and `dist` to increase as the triangles approach these limiting configurations.

The significance of the derived $C^2$ edge basis functions lies in their ability to be applied to the construction of B–spline–like bases for various $C^2$ spline spaces over general triangulations. In particular, the $C^2$ super-smooth Argyris spline space (see Fig. 1, right) represents a natural and important direction for further investigation. Another relevant class of spline spaces is the $C^2$ continuous

Clough–Tocher spline space, which is especially attractive since the requirement that neighboring triangles form a convex quadrilateral is automatically satisfied when each triangle split point is chosen as the incenter. However, a systematic treatment of these spline spaces requires addressing additional nontrivial technical issues related to the consistent combination of vertex and edge basis functions. A detailed analysis of these aspects is beyond the scope of the present paper and is therefore deferred to future research.

## 6. Notes on $C^r$ continuous B–spline–like basis functions

The functions

$$\mathcal{F} = \left\{ \varphi_{k,i}^{Q_j} \;:\; j \in \{1,2\},\, r \le k \le d-r,\, i = 1,2,\dots,r+1 \right\},$$

defined via (9) in Subsection 3.2, provide $2(d+1-2r)(r+1)$ candidates for edge B–spline–like basis splines also in the case $r > 2$. Since the required number of such splines is $(d+1-2r)(r+1) + \binom{r+1}{2}$, it follows that the degree must satisfy $d \ge \frac{5r}{2} - 1$. Recall that in the $C^2$ case with degree $d = 4$, which equals this bound, the candidate functions in $\mathcal{F}$ fail to be linearly independent. Therefore, the true lower bound on the degree $d$ must be determined independently for each value of $r$. For $r = 3$ numerical experiments indicate that the degree should satisfy $d \ge 8$. An important advantage of the proposed construction is that once the problem is resolved for the lowest admissible degree, its extension to higher degrees becomes straightforward, as already observed in the $C^1$ and $C^2$ cases.

Since spline spaces with smoothness $r \ge 3$ are of limited practical relevance and their systematic analysis would require a case-by-case investigation for each smoothness order, we have restricted our attention in this paper to the cases $r \le 2$, leaving the analysis of higher–order smoothness as a possible direction for future work.

## 7. Conclusions

The paper presents a construction and a complete analysis of $C^1$ and $C^2$ continuous edge B–spline–like basis functions of degree $d \ge 2$ and $d \ge 4$, respectively, over two triangles sharing a common edge and forming a strictly convex quadrilateral. The construction is geometrically motivated and can be carried out for arbitrary polynomial degree $d$ above a lower bound that depends on the prescribed order of smoothness, as discussed in Section 6. The construction proceeds in two steps. First, starting from two selected control triangles equipped with Bernstein basis polynomials of degree $d$, we define candidates for $C^r$ edge B–spline–like functions. These candidates are obtained by coupling, in accordance with Lemma 1, selected Bernstein basis polynomials whose coefficients associated with the triangle group are set to zero (see Figs. 6 and 7). In the second step, the candidate functions are further coupled (see Figs. 8 and 12) to obtain linearly independent splines that satisfy the desired properties.

There are, of course, many possible ways to perform these two coupling steps. The particular choices adopted in this paper are the result of extensive numerical investigations in which the quantities $\kappa_2$ and `dist` were examined over a wide range of triangle configurations. The selected couplings exhibited the most favorable behavior with respect to these measures, provided that the ordering of the triangles is chosen such that $\mu_2 \ge \mu_1$. For $C^1$ continuity, the derived basis outperforms the basis presented in [9] in most cases. To the best of our knowledge, no comparable bases exist for higher orders of smoothness, making a direct comparison in those cases unavailable.

With the presented approach, edge basis functions can also be constructed for higher orders of smoothness, since (9) provides the candidate functions for $C^r$ splines for any $r \ge 1$. However, the second coupling step requires a case-by-case treatment for each smoothness order $r$ and is therefore left as a possible direction for future work.

Further future work includes the integration of the constructed edge B–spline–like basis functions into a complete basis for selected spline spaces over a triangulation, in particular for the $C^2$ Argyris and $C^2$ Clough–Tocher spline spaces of general sufficiently high degree. While this integration is straightforward for the *edge* basis functions, it requires the completion of certain Bézier coefficient values (in the edge group) for the *vertex* basis functions obtained via the standard control triangle approach. Another goal for future work is to apply the resulting spline spaces and their associated B–spline–like bases to approximation, surface modeling, and the numerical solution of partial differential equations.

## Declaration of competing interest

The authors declare that they have no known competing financial interests or personal relationships that could have appeared to influence the work reported in this paper.

## Acknowledgements

Research on this paper has been partly supported by the research programs P1-0288 and the research grant N1-0237 by the Slovenian Research and Innovation Agency.

## Data availability

The data used in this work are fully described in the paper.

## References

[1] M. Lai, L. Schumaker, Spline Functions on Triangulations, Cambridge University Press, 2007.
[2] J. Argyris, I. Fried, D. Scharpf, The TUBA family of plate elements for the matrix displacement method, Aeronaut. J. Roy. Aeronaut. Soc. 72 (1968) 701–709.
[3] R. Clough, J. Tocher, Finite element stiffness matrices for analysis of plates in bending, in: Conf. on Matrix Methods in Structural Mechanics, Wright–Patterson Air Force Base, Ohio, 1965, pp. 515–545.
[4] M.J.D. Powell, M. Sabin, Piecewise quadratic approximations on triangles, ACM Trans. Math. Softw. 3 (1977) 316–325.
[5] H. Speleers, A new B-spline representation for cubic splines over powell–Sabin triangulations, Comput. Aided Geom. Des. 37 (2015) 42–56.
[6] H. Speleers, A normalized basis for quintic powell–Sabin splines, Comput. Aided Geom. Des. 27 (2010) 438–457.
[7] J. Grošelj, A normalized representation of super splines of arbitrary degree on powell–Sabin triangulations, BIT Numer. Math. 56 (2016) 1257–1280.
[8] J. Grošelj, Higher-degree super-smooth $C^1$ splines over a powell–Sabin refined triangulation, Math. Comput. Simul. 243 (2026) 382–406.
[9] J. Grošelj, M. Knez, A construction of edge B-spline functions for a $C^1$ polynomial spline on two triangles and its application to argyris type splines, Comput. Math. Appl. 99 (2021) 329–344.
[10] P. Dierckx, On calculating normalized powell–Sabin B-splines, Comput. Aided Geom. Des. 15 (1997) 61–78.
[11] H. Speleers, Construction of normalized B-splines for a family of smooth spline spaces over powell–Sabin triangulations, Constr. Approx. 37 (2013) 41–72.
[12] H. Speleers, A normalized basis for reduced clough–Tocher splines, Comput. Aided Geom. Des. 27 (2010) 700–712.
[13] M. Lamnii, H. Mraoui, A. Tijini, A. Zidna, A normalized basis for $C^1$ cubic super spline space on powell–Sabin triangulation, Math. Comput. Simul. 99 (2014) 108–124.
[14] A. Lamnii, M. Lamnii, H. Mraoui, A normalized basis for condensed $C^1$ powell–Sabin-12 splines, Comput. Aided Geom. Des. 34 (2015) 5–20.
[15] J. Grošelj, H. Speleers, Construction and analysis of cubic powell–Sabin B-splines, Comput. Aided Geom. Des. 57 (2017) 1–22.
[16] H. Speleers, A family of smooth quasi-interpolants defined over powell–Sabin triangulations, Constr. Approx. 41 (2015) 297–324.
[17] T. Lyche, C. Manni, H. Speleers, Construction of $C^2$ cubic splines on arbitrary triangulations, Found. Comput. Math. 22 (2022) 1309–1350.
[18] T. Lyche, G. Muntingh, B-Spline-like bases for $C^2$ cubics on the powell–Sabin 12-split, SMAI J. Comput. Math. S 5 (2019) 129–159.
[19] S. Eddargani, M. Ibáñez, A. Lamnii, M. Lamnii, D. Barrera, Quasi-interpolation in a space of $C^2$ sextic splines over powell–Sabin triangulations, Mathematics 9 (2021) 2276.
[20] L. Ramshaw, Blossoming: A Connect-the-Dots Approach to Splines, Technical Report 19, Digital Systems Research Center, Palo Alto, CA, 1987.
[21] L. Ramshaw, Blossoms are polar forms, Comput. Aided Geom. Des. 6 (1989) 323–358.
[22] S. Mann, A Blossoming Development of Splines, Synthesis Lectures on Computer Graphics and Animation, Morgan & Claypool Publishers, 2006.
[23] J. Grošelj, M. Knez, Generalized $C^1$ clough–Tocher splines for CAGD and FEM, Comput. Methods Appl. Mech. Eng. 395 (2022) 114983.